

This discussion paper is/has been under review for the journal Ocean Science (OS).
Please refer to the corresponding final paper in OS if available.

Fate of river Tiber discharge investigated through numerical simulation and satellite monitoring

R. Inghilesi¹, L. Ottolenghi², A. Orasi¹, C. Pizzi³, F. Bignami³, and R. Santoleri³

¹Institute for Environmental Protection and Research (ISPRA), Italy

²University of Roma Tre, Italy

³Institute of Atmospheric Sciences and Climate of the Italian National Research Council – Satellite Oceanography Group (ISAC/CNR-GOS), Italy

Received: 1 March 2012 – Accepted: 6 March 2012 – Published: 12 April 2012

Correspondence to: R. Inghilesi (roberto.inghilesi@isprambiente.it)

Published by Copernicus Publications on behalf of the European Geosciences Union.

OSD

9, 1599–1649, 2012

Evaluation of Tiber river pollutant dispersion in the Tyrrhenian Sea

R. Inghilesi et al.

Title Page

Abstract

Introduction

Conclusions

References

Tables

Figures

⏪

⏩

◀

▶

Back

Close

Full Screen / Esc

Printer-friendly Version

Interactive Discussion

Abstract

The aim of this study was to determine the dispersion of passive pollutants associated with the Tiber discharge into the Tyrrhenian Sea using numerical marine dispersion models and satellite data. Numerical results obtained in the simulation of realistic discharge episodes were compared with the corresponding evolution of the spatial distributions of MODIS diffuse light attenuation coefficient at 490 nm (K490), and the results were discussed with reference to the local climate and the seasonal sub-regional circulation regime. The numerical model used for the simulation of the sub-tidal circulation was a Mediterranean sub-regional scale implementation of the Princeton Ocean Model (POM), nested in the large-scale Mediterranean Forecasting System. The nesting method enabled the model to be applied to almost every area in the Mediterranean Sea and also to be used in seasons for which imposing climatological boundary conditions would have been questionable. Dynamical effects on coastal circulation and on water density due to the Tiber discharge were additionally accounted for in the oceanographic model by implementing the river estuary as a point source of a buoyant jet. A Lagrangian particle dispersion model fed with the POM current fields was then run, in order to reproduce the effect of the turbulent transport of passive tracers mixed in the plume with the coastal flow. Two significant episodes of river discharge in both Winter and Summer conditions were discussed in this paper. It was found that the Winter regime was characterized by the presence of a strong coastal jet flowing with the ambient current. In Summer the prevailing wind regime induces coastal downwelling conditions, which tend to confine the riverine waters close to the shore. In such conditions sudden wind reversals due to local weather perturbations, causing strong local upwelling, proved to be an effective way to disperse the tracers offshore, moving the plume from the coast and detaching large pools of freshwater.

Evaluation of Tiber river pollutant dispersion in the Tyrrhenian Sea

R. Inghilesi et al.

[Title Page](#)

[Abstract](#)

[Introduction](#)

[Conclusions](#)

[References](#)

[Tables](#)

[Figures](#)

[⏪](#)

[⏩](#)

[◀](#)

[▶](#)

[Back](#)

[Close](#)

[Full Screen / Esc](#)

[Printer-friendly Version](#)

[Interactive Discussion](#)



1 Introduction

Most pollution of the coastal marine environment is associated with river runoff, which carries into the sea the effects of atmospheric pollution and human urban, agricultural and industrial wastes. The effects of the so-called nonpoint sources of pollution are the presence in the water of high concentration of pathogens, oxygen-depleting nutrients and many toxic substances such as heavy metals and PCBs. The Tiber, the third longest Italian river, crosses two Italian regions well known for their agricultural and farming activities, and then flows through Rome just before entering the central Tyrrhenian Sea. Even though Tiber discharges rarely exceed $200 \text{ m}^3 \text{ s}^{-1}$ in Summer, several occurrences of rapid floods have been reported to be associated with the death of most of the fish present in the final course of the river, due to the sudden depletion of oxygen in the water. Concentrations of bacteria and viruses at the river mouth are also a matter of primary concern for public health, thus potentially affecting tourism at the many coastal resorts in the central and upper Tyrrhenian sea. It is therefore important to assess the potential impact of pollutants carried in the river's fresh waters, as well as that of the sediments transported to the marine and the coastal environment. The interaction between riverine freshwater and ambient saline water in estuaries has been studied by means of layer and primitive equation models in idealized and realistic conditions. Important aspects of the problem are the dynamics associated with the discharge of light freshwater in a denser ambient flow, the presence of currents and tides, the speed and direction of the wind, the concentration of pollutants in the river and the amount of the volumetric discharge. The first of the foregoing factors has been investigated by several authors. Generally speaking, the forcing operated by the freshwater on the ambient flow can be interpreted in terms of a classical Rossby geostrophic adjustment problem (Hsieh and Gill, 1983). As shown by Garvine (1987), rotation is a key factor in the dynamics of the plume. Even for small estuaries, the Coriolis acceleration greatly modifies the density fields and the currents at considerable distances from the river mouth. The characteristic scales of the problem are the width

Evaluation of Tiber river pollutant dispersion in the Tyrrhenian Sea

R. Inghilesi et al.

Title Page

Abstract

Introduction

Conclusions

References

Tables

Figures



Back

Close

Full Screen / Esc

Printer-friendly Version

Interactive Discussion



Evaluation of Tiber river pollutant dispersion in the Tyrrhenian Sea

R. Inghilesi et al.

[Title Page](#)[Abstract](#)[Introduction](#)[Conclusions](#)[References](#)[Tables](#)[Figures](#)[⏪](#)[⏩](#)[◀](#)[▶](#)[Back](#)[Close](#)[Full Screen / Esc](#)[Printer-friendly Version](#)[Interactive Discussion](#)

The wind rose of wind speed and direction at the meteorological station of Civitavecchia over 20 years of recordings is shown in Fig. 1. It indicates that there are two prevailing wind regimes, i.e. northeasterly winds and south-south-easterly winds. The former prevails during Winter, having the maximum of the frequency distribution in December–January, the latter dominates Summer and Autumn with maximum of the frequency distribution in Summer, but stronger winds ($>7 \text{ m s}^{-1}$) in Autumn. The northeasterly regime has winds directed seaward in the area of the river mouth, the South regime makes favorable conditions for downwelling. The circulation in the Central Tyrrhenian Sea is markedly anti-clockwise in winter, when forced by the inflows of MAW from the Western Mediterranean through the Sardinia Channel and by the Eastern Mediterranean LIW passing through the Sicily channel. In Summer and early Autumn the circulation is less definite, as the external forcing extremely is extremely reduced. In this period local wind is the main forcing of the circulation. The amplitude of the tidal cycle near the river mouth is less than 0.2 m, so only the sub-tidal circulation was considered in this study.

The dispersion of the riverine waters was studied using a three-dimensional, primitive equation, oceanographic model in the domain shown in Fig. 2, coupled with a particle Lagrangian transport model in order to simulate the transport of a passive tracer associated with the river discharge. The evolution in time of the river plume was also tracked using remote sensing observations of K490. This quantity has proven to be very effective to detect the presence of suspended matter in the upper part of the sea associated with the river plume, especially in coastal waters of type II where the remote sensing of chl signal is not a reliable indicator of the presence of river waters (Morel and Prieur, 1977). The method was tested on several key studies in Summer and Winter conditions. The comparisons of the results of numerical simulations and remote sensing observations indicate the strengths and the weaknesses of both the analyses, providing information on how to make the best use of them in the environmental monitoring.

2 Satellite and in situ data

The diffuse light attenuation coefficient at 490 nm (K490) fields at 1km resolution were obtained by processing the original L0 radiance data regarding to the MODIS AQUA platform with the standard SeaDAS software using the SeaWiFS algorithm (Mueller, 2000). K490 is a suitable tracer for riverine discharge and coastal water tracking (Big-nami et al., 2007), as it is directly related to the quantity of suspended matter in sea-water. Indeed, even though the accuracy of the estimates in Case II (turbid coastal) waters is low, the very high values of this parameter allow for a very good distinction to be made between coastal and open sea waters, in particular for tracking sediment-rich riverine plumes. Therefore, K490 is used here to evaluate the downshelf and across-shelf penetration of the buoyancy-driven coastal current under different meteorological and hydrological conditions. As regards the wind, several sources of meteorological data were available. The ISPRA tide gauge station at Civitavecchia, equipped with a standard meteorological station is a coastal station fifty kilometers to the North-West of the river mouth. The station has been recording standard meteorological data, and in particular wind at 10 m height since August 1986. The climatological analysis of the wind in the last 25 years at Civitavecchia was compared with the statistics based on the 1971–2000 records at the Fiumicino Airport weather station. The latter is a WMO reference station run by the Italian Company for Air Navigation Services (ENAV). The distributions were found to be very similar. Two years of wind data from the offshore buoy of Civitavecchia are also available from the IPRA Waves Network (RON). The offshore wind data was reduced at 10 m height following (Kourafalou et al., 1996b; Hsu, 1986). Tiber river discharge data were available at the hydrological Ripetta station, located in downtown Rome. In the final part of its course toward the Sea the Tiber bifurcates, downstream of the Ripetta station. The main part of the flow, which enters the Tyrrhenian Sea at Fiumara Grande, carries more than 9/10 of the total flow. The other branch, a small artificial channel which has its mouth further north, at Fiumicino, has not been considered here. The geographical position of the estuaries and of the meteorological stations are shown in Fig. 3.

Evaluation of Tiber river pollutant dispersion in the Tyrrhenian Sea

R. Inghilesi et al.

Title Page

Abstract

Introduction

Conclusions

References

Tables

Figures



Back

Close

Full Screen / Esc

Printer-friendly Version

Interactive Discussion



3 The implementation of the ICE-POM model

The numerical simulations of the Tyrrhenian Sea currents were made using the ISPRA Coastal and Estuarine POM (ICE-POM) model. The Princeton Ocean Model (Mellor, 2004) is a three-dimensional model which solves the primitive equation in hydrostatic and Boussinesq approximation. The grid has sigma coordinate on the vertical and is formulated on the Arakawa C-grid, following latitude and longitude on the horizontal. Despite the fact of having variable depths in the domain and vertical velocity defined on sigma-planes, sigma coordinates are especially useful in situations of complex orography, as is the case of the Tyrrhenian Sea. The numerics of the model allows the separation of fast barotropic (external) modes i.e. sea level and vertically averaged velocity, and (internal) baroclinic modes for salinity, temperature and 3-D velocity fields. The model has been one-way nested in the domain of the Mediterranean Ocean Forecasting System, (Pinardi et al., 2003; Oddo et al., 2009). The open boundaries were located in the Sicily Channel, the Sardinia Channel and the Corsica Strait, as shown in Fig. 2. The MFS analyses were kindly provided by INGV in the framework of the My-Ocean project. The nesting allows the ICE-POM to be implemented almost everywhere in the Mediterranean Sea, in any season and meteorological condition. The model grid used had 375×300 nodes with 32 sigma vertical levels. The horizontal dimension of the grid cells was close to $2.0 \times 2.0 \text{ Km}^2$. The vertical size of the cells was linear in the central 26 levels, logarithmically distributed in the top 4, and in the 2 bottom cells. The time step for the external mode was set to 6.0 s at the beginning of the spin-up period, and reduced to 1 s during discharge episodes exceeding $600 \text{ m}^3 \text{ s}^{-1}$. The ratio between external and internal mode was set to 40.

3.1 Boundary conditions

Lateral boundary conditions (BC) were imposed at the open boundaries shown in Fig. 2, while at the surface heat flux and wind stress forcing were considered. The usual condition of no fluxes, no slip velocity were applied at the bottom. Initial and

OSD

9, 1599–1649, 2012

Evaluation of Tiber river pollutant dispersion in the Tyrrhenian Sea

R. Inghilesi et al.

Title Page

Abstract

Introduction

Conclusions

References

Tables

Figures

⏪

⏩

◀

▶

Back

Close

Full Screen / Esc

Printer-friendly Version

Interactive Discussion



effects on the circulation and on the water density due to the river outflow were accounted for by considering the sub-grid river discharge as a buoyant jet-like feature in the POM (Oey, 1996). Due to the steep salinity gradients, the time step of the ICE-POM used was reduced to 1.0 s during significant discharges. The numerical scheme used for the horizontal advection was the classical centered scheme described in Mellor (2004). By reducing the time step it was possible to use the centered scheme up to discharges of the order of $1000 \text{ m}^3 \text{ s}^{-1}$, which is the order of magnitude of the maximum discharge in the Winter episode here described. In the cases of discharges above this threshold, negative salinity occurred close to the freshwater source and the central scheme had to be replaced by the Smolarkiewicz iterative upstream scheme. The latter method was used to simulate an episode of $1800 \text{ m}^3 \text{ s}^{-1}$ which occurred in December 2008 (not discussed here).

3.3 Lagrangian particle dispersion

A Lagrangian particle dispersion model was applied to the Eulerian ICE-POM velocity fields in order to reproduce the effects of the turbulent transport of passive tracers within the discharged riverine waters. The model used was developed by V. Artale and G. M. Sannino, see García Lafuente et al. (2007). Particles were advected with a 3-D second-order Runge-Kutta scheme, the stochastic contribution was a simple Random-Walk process in which the turbulent diffusivity coefficients were provided by POM by means of the Smagorinsky formulation for the horizontal diffusivity, and the Mellor-Yamada scheme for the vertical diffusivity. The same number of particles was released at every time step, but their volume was linearly weighted with the value of the daily riverine discharge, so that particles released during episodes of significant discharge contributed more than others to the evaluation of the concentrations. The particles were always non-buoyant and non-decaying, i.e. they represented a conservative tracer neutrally dispersed by the flow. The Lagrangian model was implemented on the same grid and with the same resolution as the POM, the time step used was 300 s. The simulations were made during significant river discharge episodes in both Winter

Evaluation of Tiber river pollutant dispersion in the Tyrrhenian Sea

R. Inghilesi et al.

Title Page

Abstract

Introduction

Conclusions

References

Tables

Figures



Back

Close

Full Screen / Esc

Printer-friendly Version

Interactive Discussion



Evaluation of Tiber river pollutant dispersion in the Tyrrhenian Sea

R. Inghilesi et al.

Title Page

Abstract

Introduction

Conclusions

References

Tables

Figures

⏪

⏩

◀

▶

Back

Close

Full Screen / Esc

Printer-friendly Version

Interactive Discussion



month of January. The plume assumed a more or less stationary configuration after the first week of simulation. The numerical simulations for the 10th January are in agreement with the known features of the Tyrrhenian Sea in the Winter season. That is, in Fig. 8 the surface temperature map indicates the presence of a strong and widespread gyre near the Bonifacio Strait between Sardinia and Corsica. The MAW inflow from the western open boundary is visible in surface salinity (Fig. 6). The LIW inflow in the Tyrrhenian Sea follows the relatively deep (600 m) trench in the Sicily channel, as visible in Fig. 7 and Fig. 9. As shown in Fig. 5, the ambient current northwest off the river mouth formed a strong jet which ran at the border of the cyclonic vortex, reaching 0.9 m s^{-1} not far from the eastern coast. Outside of the jet, the current nearshore was around $0.1\text{--}0.3 \text{ m s}^{-1}$. The river plume, well visible in surface salinity (Fig. 6), 'hugged' the coast, except where the strong jet met the plume. Two days later, the jet was able to detach the plume from the coast, as shown in Fig. 11.

The 12 January situation can be described in the light of the wind conditions, satellite data and model output. The starting conditions were characterized by prevailing southerly wind conditions. The K490 map for 12 January (Fig. 4) shows that the Tiber plume had a substantial bulge northwest of the river mouth. Despite the presence of clouds, a northwestward directed jet is clearly visible along the coast. The width of the jet, which exhibited a significant meander as distance from its source increased, was smaller than the size of the bulge at the mouth, indicative of a supercritical regime. South of the Tiber mouth the presence of a weaker coastal plume was also visible (Fig. 4), probably issuing from the coastal lakes and canals of Sabaudia (80 Km south of the Tiber mouth, not shown). Further offshore a westward propagation of coastal waters was observed in the north, between S. Marinella and Argentario, though with lower K490 values (0.40 m^{-1}) than those of the coastal strip ($0.50\text{--}0.60 \text{ m}^{-1}$).

The POM current field in the Tiber area was directed offshore near the coast and formed a westward jet, in agreement with the K490 pattern (see also Fig. 11) embedded in the strong current directed towards the Corsica Channel. The POM salinity field indicates that the jet was composed of low salinity water issuing from the

Evaluation of Tiber river pollutant dispersion in the Tyrrhenian Sea

R. Inghilesi et al.

[Title Page](#)[Abstract](#)[Introduction](#)[Conclusions](#)[References](#)[Tables](#)[Figures](#)[⏪](#)[⏩](#)[◀](#)[▶](#)[Back](#)[Close](#)[Full Screen / Esc](#)[Printer-friendly Version](#)[Interactive Discussion](#)

riverine-coastal patch. In addition, the low salinity of the jet was caused by Tiber water, given the fact that only the Tiber was imposed as freshwater source in the model. The results of the Lagrangian particle model for 12 January (Fig. 12) indicate that most of the particle concentration was bounded near the shore both north and south of the river mouth. However, to the north of the Tiber mouth, some particles followed the westward low salinity jet seen in the POM salinity and in the K490 map. Finally, the differences in shape between the low salinity and particle distributions indicate that the Lagrangian model was able to detect the presence of large pools of particles detaching from the mean stream, but there is a definite indication that the plume of particles is more concentrated than the plume of freshwater. This can be related to the small value of the horizontal diffusivity generated by ICE-POM.

The presence of riverine waters south of the Tiber mouth could be due to the preceding episode of strong discharge occurred on the 8 January. In such conditions the plume might have been characterized by a subcritical regime. Both the tau and lambda estimates suggest that the plume was supercritical on the 12th, when the discharge had returned to be close to the monthly average value. The effect of the seaward wind in the first decade of January was to direct the freshwater transport towards the shelf break, but also to induce a coastal Ekman current directed against the ambient circulation, also possibly related to the presence of riverine waters south of the estuary (Chao, 1988).

On 16 January, the K490 map in Fig. 13 shows lower values in the coastal area than on 12 January, as well as a reduced width of the river jet-bulge system. This is due in part to the decrease of the discharge, passing from a maximum of $1187 \text{ m}^3 \text{ s}^{-1}$ recorded on the 8th to $300 \text{ m}^3 \text{ s}^{-1}$ a week later, but also to the rotation of the wind to southerly (downwelling) in the period from the 13th to the 15th. A similar transition of the wind from seaward to landward occurred the 21th, affecting the width of the bulge/plume system some days later, as can be seen comparing the K490 maps of the 19th, Fig. 14, and of the 22nd, Fig. 15.

The results of the Lagrangian particle model for the 12 January are shown in Fig. 12. It is apparent that most of the particle concentration is bounded near the shore both to the north and to the south of the river mouth. The plume was detached from the coastline downstream, forming an isolated filament.

4.2 Summer episode

The period 1 July–6 August 2010 was characterized by changes in the the wind regime, which, while downwelling-favorable for most of the time, changed to upwelling-favorable on two separate occasions. The recordings of the ISPRA RON (offshore) and RMN (onshore) meteorological stations of Civitavecchia clearly indicated how indicated how, from the beginning to mid July, a classical sea breeze superimposed upon the dominant Summer wind regime, the latter being a prevailing southerly wind. The first episode of northwesterly (upwelling) wind occurred between the 16 and 18 July (Fig. 16). During the following week the prevailing southerlies resumed; then, from the 24th to the 26th (Fig. 17) the wind once again was directed northerly or northwesterly.

It turned then southerly on the 27th, but rotated northerly from 31 July to 2 August (Fig. 18). Wind speed was almost always less than 8 m s^{-1} . The discharge in the period was feeble, the monthly average was around $141 \text{ m}^3 \text{ s}^{-1}$ with only a weak peak of $217 \text{ m}^3 \text{ s}^{-1}$ on 31 July. The ICE-POM spin-up was started on 22 June and was carried out for ten days. The particles were released from 2 July until the end of the simulation on 8 August. The coastal current in the period was weak and dominated by the presence of a number of gyres, in particular in the southern part of the domain (not shown). On the 14 July the circulation in the northern part of the Tyrrhenian Sea was affected by the presence of the cyclonic vortex near the Bonifacio Strait as shown in Fig. 20, reduced in size and vertically stretched with respect to the Winter key-study. This situation has been also described in Artale et al. (1994). The gyre was surrounded by anti-cyclonic structures inducing a northward coastal current along the coast of Sardinia and Corsica on the western boundary and a southeastward current on the Eastern boundary.

Evaluation of Tiber river pollutant dispersion in the Tyrrhenian Sea

R. Inghilesi et al.

Title Page

Abstract

Introduction

Conclusions

References

Tables

Figures

⏪

⏩

◀

▶

Back

Close

Full Screen / Esc

Printer-friendly Version

Interactive Discussion



The Summer episode can be described using satellite and numerical hindcast as follows.

In the period 12–14 of July the surface wind recorded onshore was about 5 m s^{-1} and southerly (Fig. 17). Such conditions were favorable to downwelling of the coastal waters. As shown in Fig. 22, the river plume was close to the shore, both north and south of the river mouth. The Lagrangian particle model confirms that the riverine water was confined close to the shore, the pattern of particle concentration, visible in Fig. 21, showing high concentrations north of the river mouth and a filament of previously emitted particles carried southeastwards. From 16 to 18 the wind turned northwesterly with speed (offshore) around $5\text{--}6 \text{ m s}^{-1}$, creating the conditions for a moderate upwelling. In Fig. 23 the effect of upwelling is evident. Comparison between the two surface salinity maps for the 14th (Fig. 20) and 18th (Fig. 24), shows the effects of upwelling occurring along the shore both north and south of the river mouth. On the 18th the map of particle concentrations generated by the Lagrangian model (Fig. 25) closely matches the K490 features, shown in Fig. 23, in the coastal area and south of the river mouth, but the northwestward particle (Tiber) filament is not seen in the K490 image, which instead shows a filament of coastal origin propagating southeastwards.

From 19th to 24th the southerly Summer regime prevailed (Fig. 17), with low winds inducing downwelling conditions. As shown in Fig. 26 and Fig. 27, the river plume recently generated was confined nearshore, while offshore, the remainder of the previous discharge was fading. In the following days, from 24 to 27 July, the wind rotated, keeping between northwesterly and northerly for 3 days with speed (offshore) exceeding 6 m s^{-1} (see Fig. 19). In this period the wind was often parallel to the coastal current and favorable to the upwelling of coastal waters south of the river mouth. The K490 image on 27 July (Fig. 28) shows that the plume had reached far offshore. The formation of strong upwelling conditions near the Tiber mouth induced by the northwesterly wind, can be inferred from the map of salinity (Fig. 29). Particle concentrations shown in Fig. 30, are similar to the K490 distribution in Fig. 28 near shore, with a large pool of particles emitted during the the preceding days being carried away southeastwards.

Evaluation of Tiber river pollutant dispersion in the Tyrrhenian Sea

R. Inghilesi et al.

Title Page

Abstract

Introduction

Conclusions

References

Tables

Figures



Back

Close

Full Screen / Esc

Printer-friendly Version

Interactive Discussion



A similar situation occurred at the beginning of August, as can be seen in Fig. 31. The transition from downwelling to upwelling was examined in an idealized numerical experiment by García Berdeal et al. (2002), and, in fact, the maps of K490 in Fig. 23, Figs. 28 and 31 agreed closely with their findings.

5 Conclusions

The implementation of a three-dimensional, high resolution, vertical sigma coordinate model on the Tyrrhenian Sea was effective in reproducing the features of the circulation both in Winter and Summer conditions, as results from the comparison with MODIS diffuse light attenuation coefficient (K490) images. The Tiber river discharge was simulated as a point source of a buoyant plume. This simplified implementation gave satisfactory results in reproducing the main features of the river plume in different environmental conditions. The use of numerical simulations and satellite maps of K490 led to the identification of different conditions of discharge, e.g. supercritical plumes for discharges indicatively smaller than $1000 \text{ m}^3 \text{ s}^{-1}$, possibly subcritical for discharges exceeding this value. On the basis of information concerning the local climatic regimes of wind and currents, the main characteristics of the dispersion of the Tiber freshwater and the tracers associated with it can be identified. In winter, due to the prevailing seaward wind regime and the ambient currents directed northwestward, the plume “hugs” the coast, forming a well-defined coastal jet directed downstream. Occasionally, when the wind turns northerly or northwesterly, upwelling may occur, with the wind blowing against the direction of the local current, and possibly reducing the strength of the coastal jet. In Summer the wind regime is Southerly most of the time, creating favorable conditions for downwelling. The local current is dominated by the presence of gyres and is not as regular and steady as in Winter. In the Summer episode considered the current was initially directed southward, against the direction of the wind. This condition led to a confinement of the freshwater of the plume near the river mouth. The subsequent turning of the wind to northwesterly allowed upwelling on three distinct

Evaluation of Tiber river pollutant dispersion in the Tyrrhenian Sea

R. Inghilesi et al.

Title Page

Abstract

Introduction

Conclusions

References

Tables

Figures



Back

Close

Full Screen / Esc

Printer-friendly Version

Interactive Discussion



Evaluation of Tiber river pollutant dispersion in the Tyrrhenian Sea

R. Inghilesi et al.

[Title Page](#)[Abstract](#)[Introduction](#)[Conclusions](#)[References](#)[Tables](#)[Figures](#)[Back](#)[Close](#)[Full Screen / Esc](#)[Printer-friendly Version](#)[Interactive Discussion](#)

occasions, with wind blowing parallel to the ambient current. On these occasions the plume detached from the coast and, some days later, created large pools of freshwater which, eventually, became dispersed. Generally, in Winter, the coastal jet is effective in dispersing pollutants downstream along the shoreline. A turning of wind conditions towards those favorable to downwelling, or the occurrence of rough sea, could have been important factors in forcing the tracers toward the coasts. In Summer, due to the prevailing southerly wind regime, the conditions for a significant containment of the tracers near the shore occur frequently. As the Tiber discharges are weaker in this season than in the rest of the year, high concentrations of pollutants are likely to be found close to its mouth after the occasional increased runoffs. The main problem in the use of satellite data is the small number of maps available during Winter. Nevertheless, the analysis of numerical simulations of the river plume carried out here proved capable of overcoming this limitation, by highlighting the temporal evolution of the flow. In this framework the K490 maps were found to be extremely important for the understanding of the main processes associated with the plume dynamics.

Acknowledgements. The authors are deeply indebted to Vincenzo Artale, Adriana Carillo and Gianmaria Sannino of ENEA for their many important suggestions concerning the use of POM and for making their Lagrangian particle model available. This work would not have been possible without their full support. Our thanks to Barbara Lastoria of ISPRA for providing and checking the Tiber hydrological data. Many thanks to the INGV and especially to Nadia Pinardi for making available the Mediterranean Forecasting System analysis.

References

- Artale, V., Astraldi, M., Buffoni, G., and Gasparini, P.: Seasonal variability of gyre-scale circulation in the northern Tyrrhenian Sea, *J. Geophys. Res.*, 99, 127–137, 1994. 1611
- Astraldi, M. and Gasparini, G. P.: The seasonal Characteristics of the Circulation in the North Mediterranean Basin and Their Relationship With the Atmospheric-Climatic Conditions, American Geophysical Union, 92JC00114, 9531–9540, 1992.
- Bargagli, A., Carillo, A., Pisacane, G., Ruti, P. M., Struglia, M. V., and Tartaglione, N.: An integrated forecast system over the Mediterranean Basin: Extreme surge prediction in the Northern Adriatic Sea. *Mon. Wea. Rev.*, 130, 1317–1332, 2022. 1606
- Bignami, F., Sciarra, R., Carniel, S., and Santoleri, R.: Variability of Adriatic Sea coastal turbid waters from SeaWiFS imagery, *J. Geophys. Res.*, 112, C03S10, 2007. 1604
- Buongiorno Nardelli, B., Tronconi, C., and Santoleri, R.: High and Ultra-High resolution processing of satellite Sea Surface Temperature data over the Southern European Seas in the framework of MyOcean project, paper submitted to *Rem. Sens. Env.*, 2011. 1606
- Blumberg, A. F. and Mellor, G. L.: A Description of a Three-Dimensional Coastal Ocean Circulation Model, reprinted from *Three Dimensional Coastal Ocean Models* by N. S. Heaps (Editor), American Geophysical Union, Washington DC, 1–16, 1987.
- Capelli, G., Mazza, R., and Papiccio, C.: Intrusione salina nel Delta del Fiume Tevere. *Geologia, idrologia e idrogeologia del settore romano della piana costiera*, *Giornale di Geologia Applicata*, 5, 13–28, 2007. 1606
- Buzzi, A., Fantini, M., Malguzzi, P., and Nerozzi, F.: Validation of a limited area model in cases of Mediterranean cyclogenesis: surface fields and precipitation scores, *Meteorol. Atmos. Phys.*, 53, 137–153, 1994. 1606
- Chao, S. Y.: River-Forced Estuarine Plumes, *J. Phys. Oceanogr.*, 18, 1–17, 1987. 1602
- Chao, S. Y.: Wind-Driven Motion of Estuarine Plumes, 18, 1–23, 1988. 1602, 1610
- Dobricic, S., Pinardi, N., Adani, M., Bonazzi, A., Fratianni, C., Tonani, M.: Mediterranean Forecasting System: an imprecise assimilation scheme for sea-level anomaly and its validation, *Q. J. R. Meteorol. Soc.*, 131, 3627–3642, 2005.
- Ezer, T. and Mellor, G. L.: Sensitivity studies with the North Atlantic sigma coordinate Princeton Ocean Model, *Dynamics of Atmospheres and Oceans*, 32, 185–208, 1999.
- Fong, D. A. and Geyer, W. R.: Response of a river plume during an upwelling favorable wind event, *J. Geophys. Res.*, 106, 1067–1084, 2001. 1602

Evaluation of Tiber river pollutant dispersion in the Tyrrhenian Sea

R. Inghilesi et al.

Title Page

Abstract

Introduction

Conclusions

References

Tables

Figures

⏪

⏩

◀

▶

Back

Close

Full Screen / Esc

Printer-friendly Version

Interactive Discussion



Evaluation of Tiber river pollutant dispersion in the Tyrrhenian Sea

R. Inghilesi et al.

Title Page

Abstract

Introduction

Conclusions

References

Tables

Figures

⏪

⏩

◀

▶

Back

Close

Full Screen / Esc

Printer-friendly Version

Interactive Discussion



- García Berdeal, I., Hickey, B. M., and Kawase, M.: Influence of Wind Stress and Ambient Flow on a High Discharge River Plume, *J. Geophys. Res.*, 107, 3030–3050, 2002. 1602, 1613
- García Lafuente, J., Sánchez Román, A., Díaz del Río, G., Sannino, G., Sánchez Garrido, J. C.: Recent observations of seasonal variability of the Mediterranean outflow in the Strait of Gibraltar, *J. Geophys. Res.*, 112, C10005, 2007. 1607
- Garvine, R. W.: Estuary Plumes and Fronts in Shelf Waters: A Layer Model. *J. Phys. Oceanogr.*, 1877–1896, 1987. 1601, 1602
- Hsieh, W. W. and Gill, A. E.: The Rossby Adjustment Problem in Rotating, Stratified Channel, with and without Topography, *J. Phys. Oceanogr.*, 1–14, 1983. 1601
- Hsu, S. A.: A Mechanism for the Increase of Wind Stress (Drag) Coefficient with Wind Speed over Water Surfaces: A Parametric Model, *J. Phys. Oceanogr.*, 144–150, 1986. 1604
- Leuzzi, G. and Monti, P.: The coupling of POM with a lagrangian, first order, auto regressive dispersion model, atti del 5th International Symposium on Environmental Hydraulics, 4–7 December, Tempe, AZ, 2007.
- Kourafalou, V. H., Oey, L. Y., Wang, J. D., and Lee, T. N.: The fate of river discharge on the continental shelf 1. Modeling the river plume and the inner shelf coastal current. *J. Geophys. Res.*, 101, 3415–3434, 1996. 1602
- Kourafalou, V. H., Oey, L. Y., Wang, J. D., and Lee, T. N.: The fate of river discharge on the continental shelf 2. Transport of coastal low-salinity waters under realistic wind and tidal forcing, *J. Geophys. Res.*, 101, 3435–3455, 1996. 1604
- Mellor, G. L.: Users guide for a three-dimensional, primitive equation, numerical ocean model, 2004. 1605, 1607
- Mellor, G. L. and Jamada, T.: A Hierarchy of Turbulence Closure Models for Planetary Boundary Layers, *J. Atmos. Sci.*, 31, 1791–1806, Corrigendum, 34, 1482, 1974. 1606
- Menzel, W. P.: Remote sensing applications with meteorological satellites, NOAA Satellite and Information Service, University of Wisconsin, Madison, WI, 2006.
- Millot, C.: Circulation in the Western Mediterranean Sea, *J. Mar. Syst.*, 20, 423–442, 1999.
- Millot, C. and Taupier-Letage, I.: Circulation in the Mediterrean Sea, *The Handbook of Environmental Chemistry, Vol. 1 (The Natural Environment and the Biological Cycles)*, Springer-Verlag, 2004.
- Mobley, C. D., Stramsky, D., Bisset, W. P., and Boss, E.: Optical modeling of ocean waters. Is the Case 1- Case 2 classification still usefull?, *Oceanography*, 17, 60–67, 2004.
- Morel, A., Prieur, L.: Analysis of variations in ocean color, *Limnology and Oceanography*, 22,

Evaluation of Tiber river pollutant dispersion in the Tyrrhenian Sea

R. Inghilesi et al.

[Title Page](#)

[Abstract](#)

[Introduction](#)

[Conclusions](#)

[References](#)

[Tables](#)

[Figures](#)

[⏪](#)

[⏩](#)

[◀](#)

[▶](#)

[Back](#)

[Close](#)

[Full Screen / Esc](#)

[Printer-friendly Version](#)

[Interactive Discussion](#)

709–722, 1977. 1603

Oey, L. Y. and Mellor, G. L.: Subtidal Variability of Estuarine Outflow, Plume and Coastal Current: A Model Study. *J. Phys. Oceanogr.*, 23, 1–8, 1992.

5 Oddo, P., Adani, M., Pinardi, N., Fratianni, C., Tonani, M., and Pettenuzzo, D.: A nested Atlantic-Mediterranean Sea general circulation model for operational forecasting, *Ocean Sci.*, 5, 461–473, doi:10.5194/os-5-461-2009, 2009. 1605

Oey, L. Y.: Simulation of Mesoscale Variability in the Gulf of Mexico: Sensitivity Studies, Comparison with Observations, and Trapped Wave Propagation, *J. Phys. Oceanogr.*, 26, 145–175, 1996. 1602, 1607

10 Palma, E. D. and Matano, R. P.: Dynamical impacts associated with radiation boundary conditions, *J. Sea Res.*, 46, 117–132, 2001. 1606

Pinardi, N., Allen, I., Demirov, E., De Mey, P., Korres, G., Lascaratos, A., Le Traon, P.-Y., Maillard, C., Manzella, G., and Tziavos, C.: The Mediterranean ocean forecasting system: first phase of implementation (1998-2001), *Ann. Geophys.*, 21, 3–20, doi:10.5194/angeo-21-3-2003, 2003. 1605

15 Pinardi, N. and Masetti, E.: Variability of the large scale general circulation of the Mediterranean Sea from observations and modelling: a review, *Palaeogeogr. Palaeoclimatol.*, 158 pp., 153–173, 2000. 1606

Santoleri, R., Volpe, G., Marullo, S., and Buongiorno Nardelli, B.: Open Waters Optical Remote Sensing of the Mediterranean Sea, *J. Geophys. Res.*, 108, 1–14, 2003.

20 Sciarra, R., Böhm, E., D’Acunzio, E., and Santoleri, R.: The large scale observing system component of ADRICOSM: the satellite system, *Acta Adriatica*, 47(Suppl.), 51–64, 2006.

Serravall, R. and Cristofalo, G. C.: On the presence of a coastal current of Levantine intermediate water in the central Tyrrhenian Sea, *Ocean. Ac.*, 22, 281–290, 1999.

25 Speranza, A., Accadia, C., Casaioli, M., Mariani, S., Monacelli, G., Inghilesi, R., Tartaglione, N., Ruti, P. M., Carillo, A., Bargagli, A., Pisacane, G., Valentinotti, F., and Lavagnini, A.: POSEIDON: An integrated system for analysis and forecast of hydrological, meteorological and surface marine fields in the Mediterranean area, *Nuovo Cimento*, 27C(4), 329–345, 2004. 1606

30 Vetrano, A., Gasparini, G. P., Molcard, R., and Astraldi, M.: Water flux estimates in the central Mediterranean Sea from an inverse box model, *J. Geophys. Res.*, 109, C01019, 2004. 1606

Volpe, G., Santoleri, R., Vellucci, V., Ribera d’Alcalá, M., Marullo, S., and D’Orenzio, F.: The colour of the Mediterranean Sea: Global versus regional bio-optical algorithms evaluation

and implication for satellite chlorophyll estimates, *Remote Sens. Environ.*, 107, 625–638, 2007.

Volpe, G., Banzon, V. F., Evans, R. H., Santoleri, R., Mariano, A. J., and Sciarra, R.: Satellite observations of the impact of dust in a low-nutrient, low-chlorophyll region: fertilization or artifact?, *Global Biogeochem. Cy.*, 23, GB3007, 2009.

Xing, J. and Davies, A. M.: The effect of wind direction and mixing upon the spreading of a buoyant plume in a non-tidal regime, *Cont. Shelf Res.*, 1437–1483, 1999.

Yanovsky, A. E. and Chapman, D. C.: A Simple Theory for the Fate of Buoyant Coastal Discharges, *J. Phys. Oceanogr.*, 1386–1401, 1997.

OSD

9, 1599–1649, 2012

Evaluation of Tiber river pollutant dispersion in the Tyrrhenian Sea

R. Inghilesi et al.

Title Page

Abstract

Introduction

Conclusions

References

Tables

Figures

⏪

⏩

◀

▶

Back

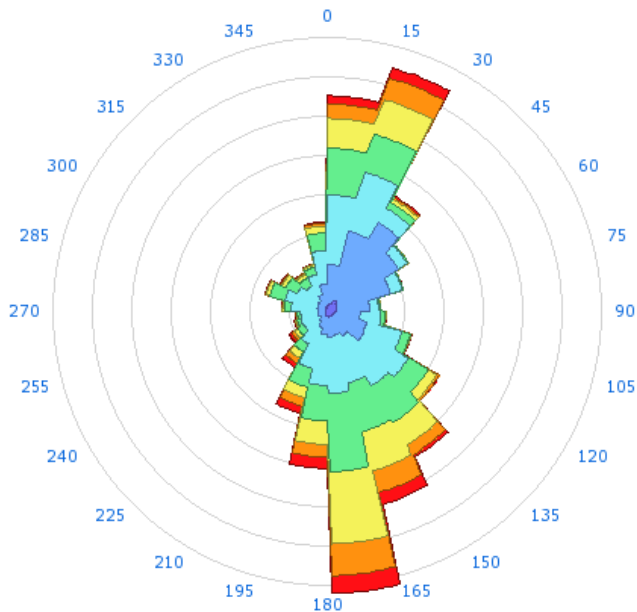
Close

Full Screen / Esc

Printer-friendly Version

Interactive Discussion





by APAT - Servizio Mareografico - www.IDROMARE.com

Fig. 1. Wind rose at Civitavecchia.

Evaluation of Tiber river pollutant dispersion in the Tyrrhenian Sea

R. Inghilesi et al.

Title Page	
Abstract	Introduction
Conclusions	References
Tables	Figures
◀	▶
◀	▶
Back	Close
Full Screen / Esc	
Printer-friendly Version	
Interactive Discussion	





Fig. 2. Red box: domain of the numerical simulation. Open boundaries are in black.

OSD

9, 1599–1649, 2012

Evaluation of Tiber river pollutant dispersion in the Tyrrhenian Sea

R. Inghilesi et al.

Title Page

Abstract

Introduction

Conclusions

References

Tables

Figures

⏪

⏩

◀

▶

Back

Close

Full Screen / Esc

Printer-friendly Version

Interactive Discussion



OSD

9, 1599–1649, 2012

Evaluation of Tiber river pollutant dispersion in the Tyrrhenian Sea

R. Inghilesi et al.

Title Page

Abstract

Introduction

Conclusions

References

Tables

Figures

⏪

⏩

◀

▶

Back

Close

Full Screen / Esc

Printer-friendly Version

Interactive Discussion

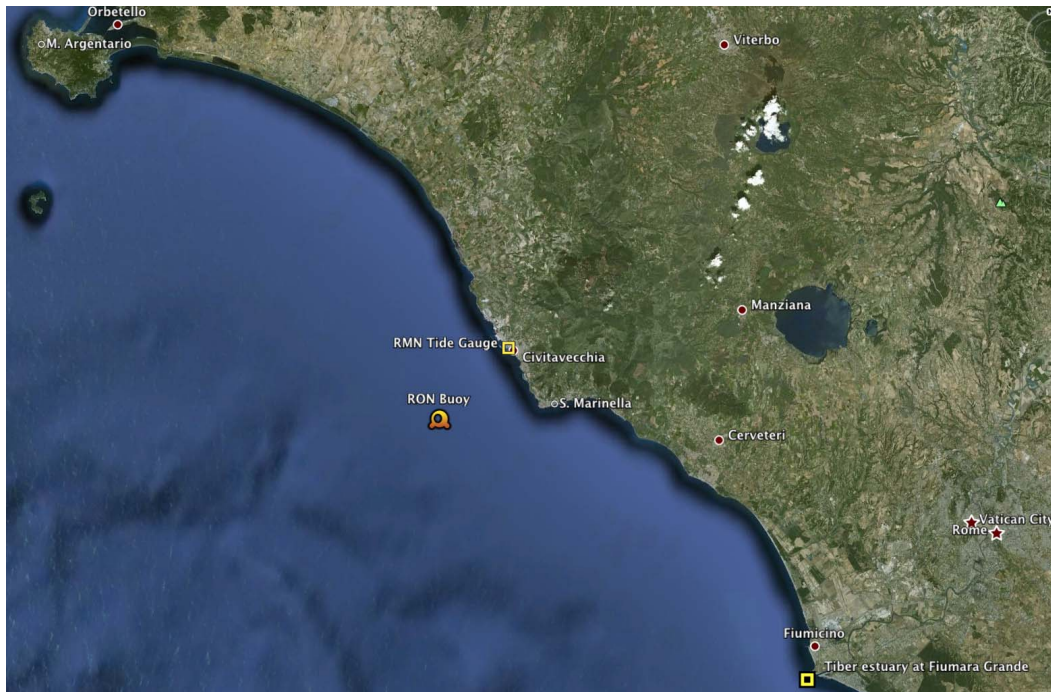
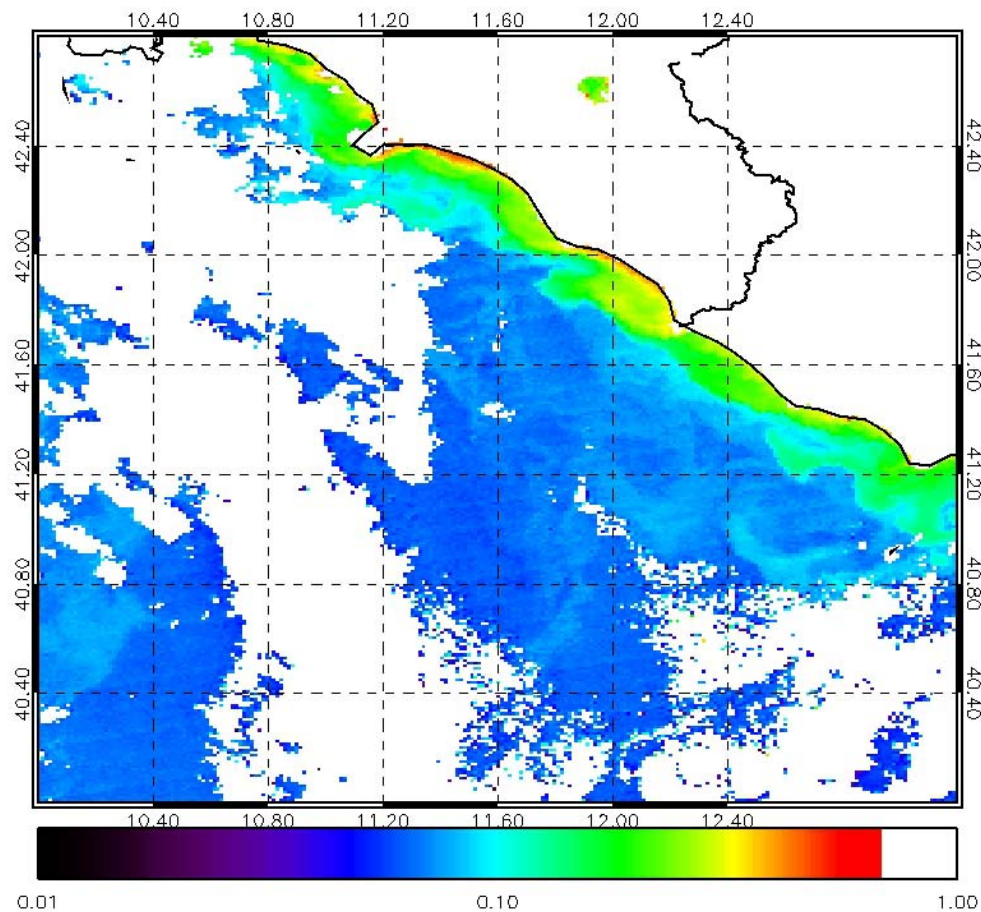


Fig. 3. Map of the shoreline North of the Tiber Estuary. The positions of the meteorological onshore and offshore stations are also indicated.

Evaluation of Tiber river pollutant dispersion in the Tyrrhenian Sea

R. Inghilesi et al.

[Title Page](#)[Abstract](#)[Introduction](#)[Conclusions](#)[References](#)[Tables](#)[Figures](#)[Back](#)[Close](#)[Full Screen / Esc](#)[Printer-friendly Version](#)[Interactive Discussion](#)**Fig. 4.** 12 January 2010, K490 coefficient.

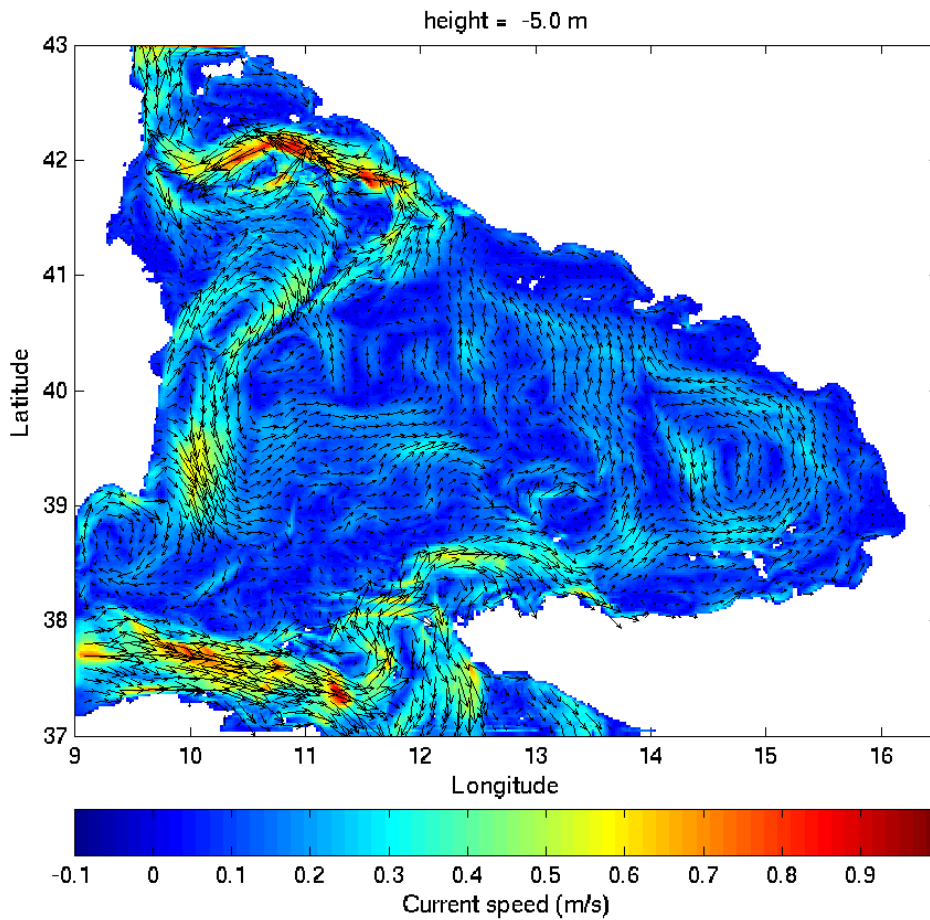


Fig. 5. 10 January 2010, current velocity at 5 m.

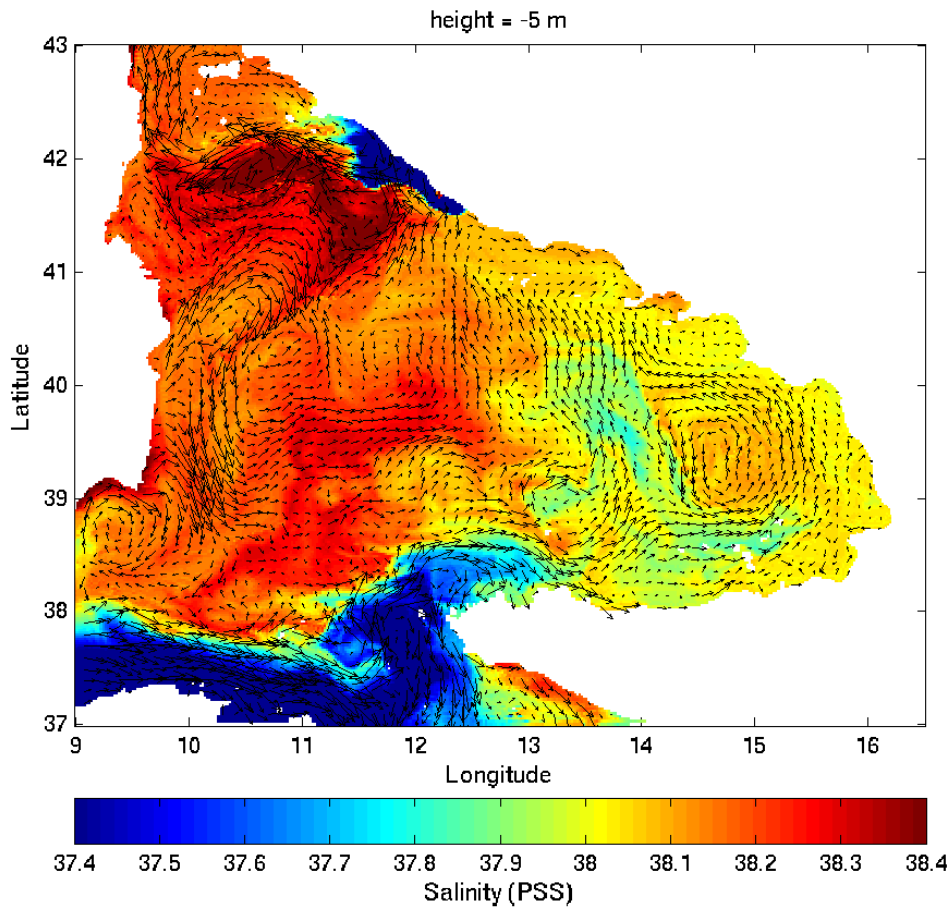


Fig. 6. 10 January 2010, salinity at 5 m.

Evaluation of Tiber river pollutant dispersion in the Tyrrhenian Sea

R. Inghilesi et al.

Title Page

Abstract	Introduction
Conclusions	References
Tables	Figures
◀	▶
◀	▶
Back	Close
Full Screen / Esc	
Printer-friendly Version	
Interactive Discussion	



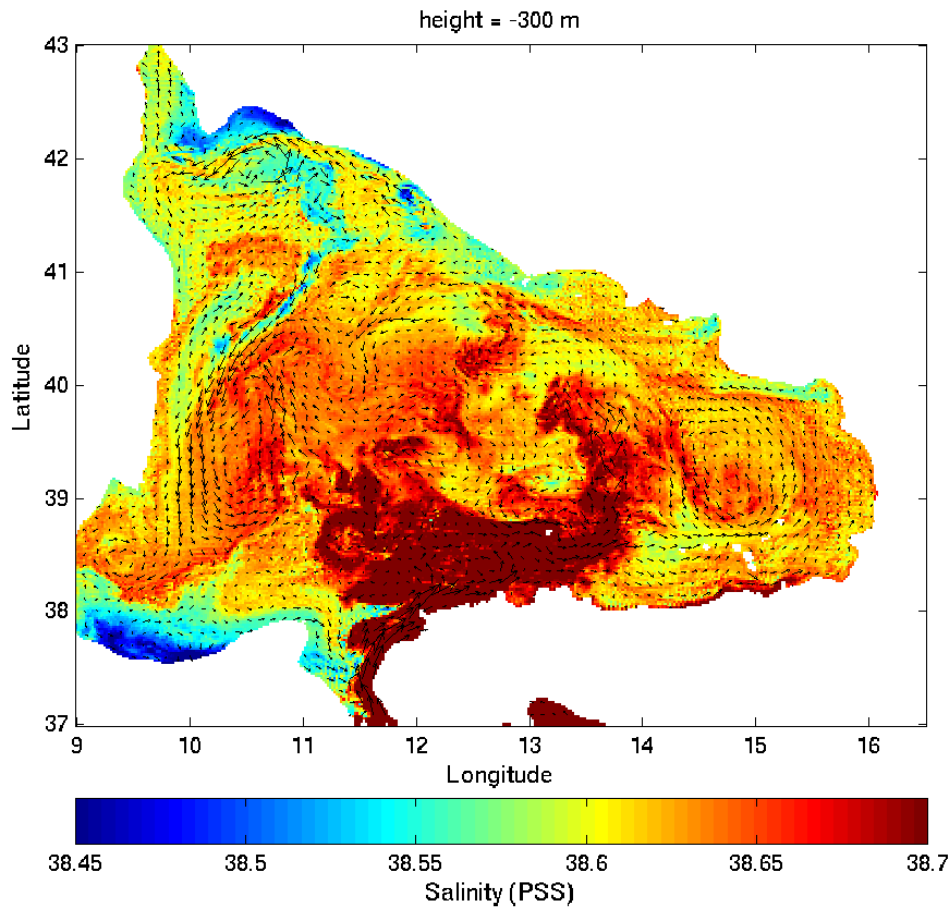


Fig. 7. 10 January 2010, salinity at 300 m.

Evaluation of Tiber river pollutant dispersion in the Tyrrhenian Sea

R. Inghilesi et al.

Title Page	
Abstract	Introduction
Conclusions	References
Tables	Figures
◀	▶
◀	▶
Back	Close
Full Screen / Esc	
Printer-friendly Version	
Interactive Discussion	



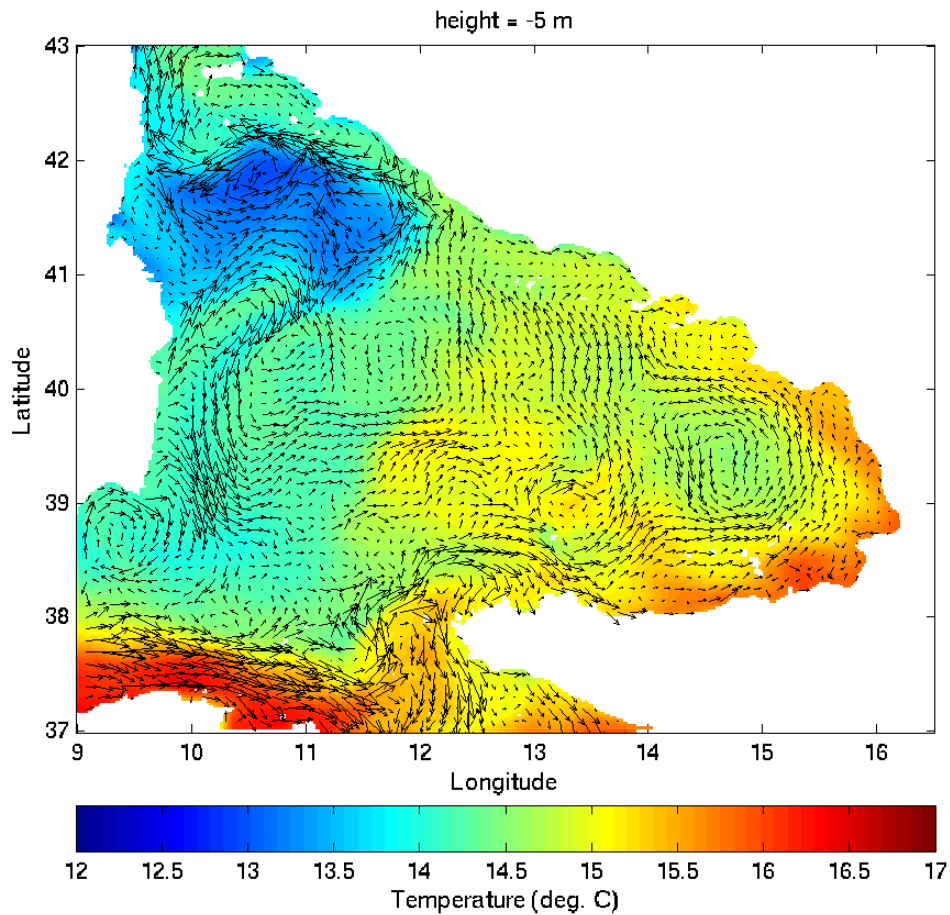


Fig. 8. 10 January 2010, temperature at 5 m.

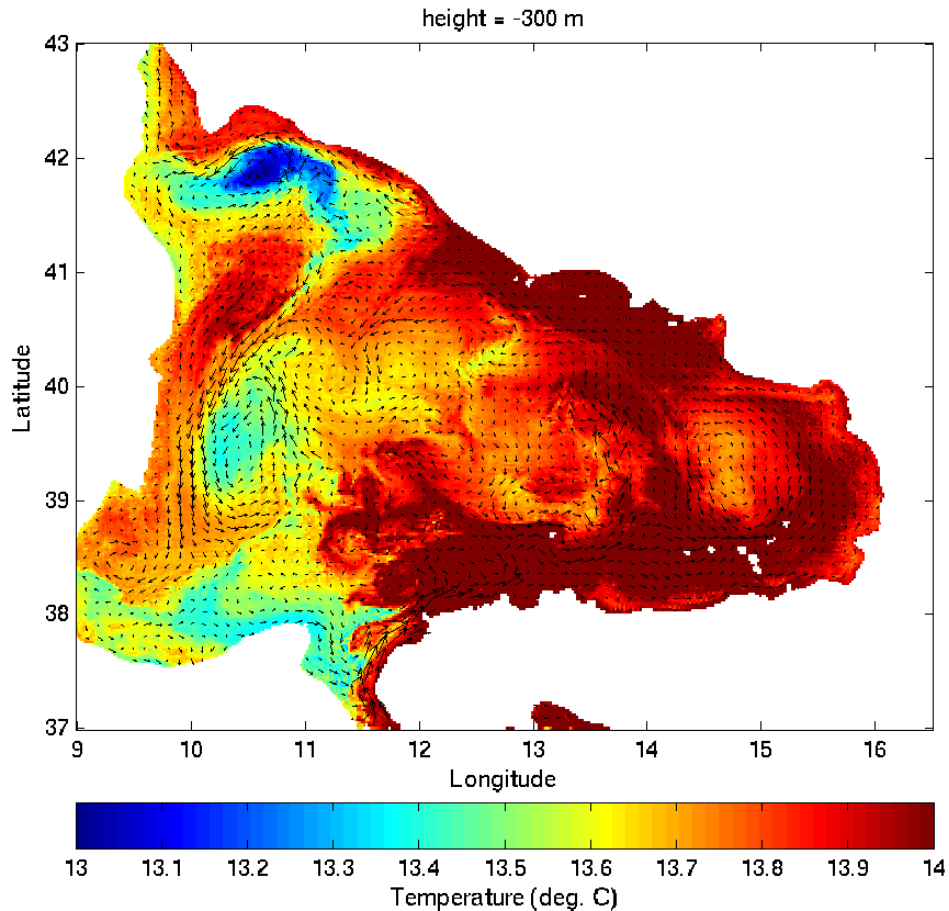


Fig. 9. 10 January 2010, temperature at 300 m (temperature scale is expanded with respect to 5 m salinity maps).

Evaluation of Tiber river pollutant dispersion in the Tyrrhenian Sea

R. Inghilesi et al.

Title Page

Abstract Introduction

Conclusions References

Tables Figures

⏪ ⏩

◀ ▶

Back Close

Full Screen / Esc

Printer-friendly Version

Interactive Discussion



Evaluation of Tiber river pollutant dispersion in the Tyrrhenian Sea

R. Inghilesi et al.

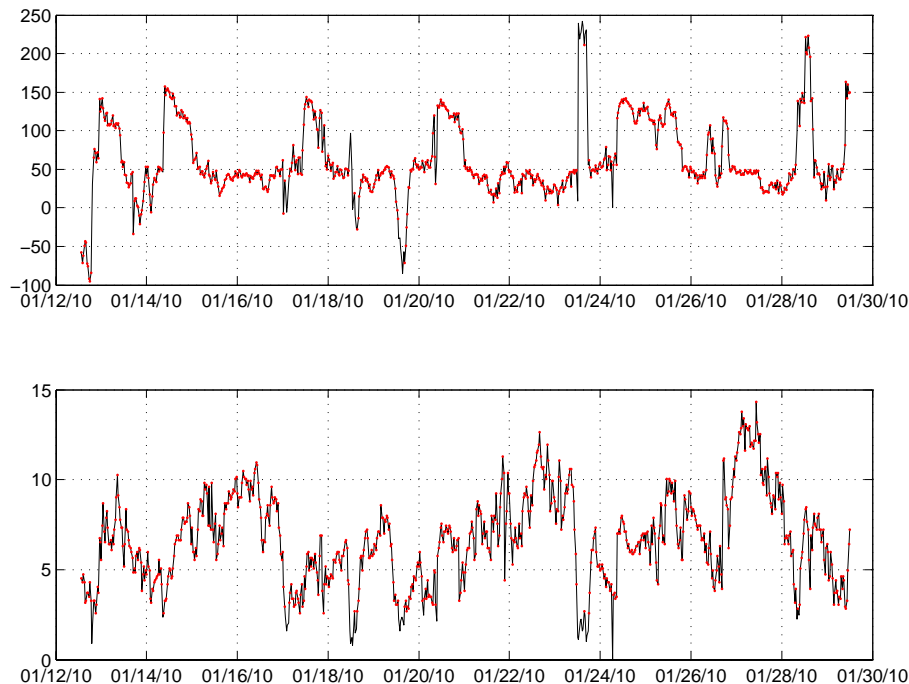


Fig. 10. Wind recorded at the RON buoy of Civitavecchia 16–28 January. **(a)** wind direction **(b)** wind speed red dots indicate wind speed greater than 2.5 m s^{-1} .

[Title Page](#)[Abstract](#)[Introduction](#)[Conclusions](#)[References](#)[Tables](#)[Figures](#)[◀](#)[▶](#)[◀](#)[▶](#)[Back](#)[Close](#)[Full Screen / Esc](#)[Printer-friendly Version](#)[Interactive Discussion](#)

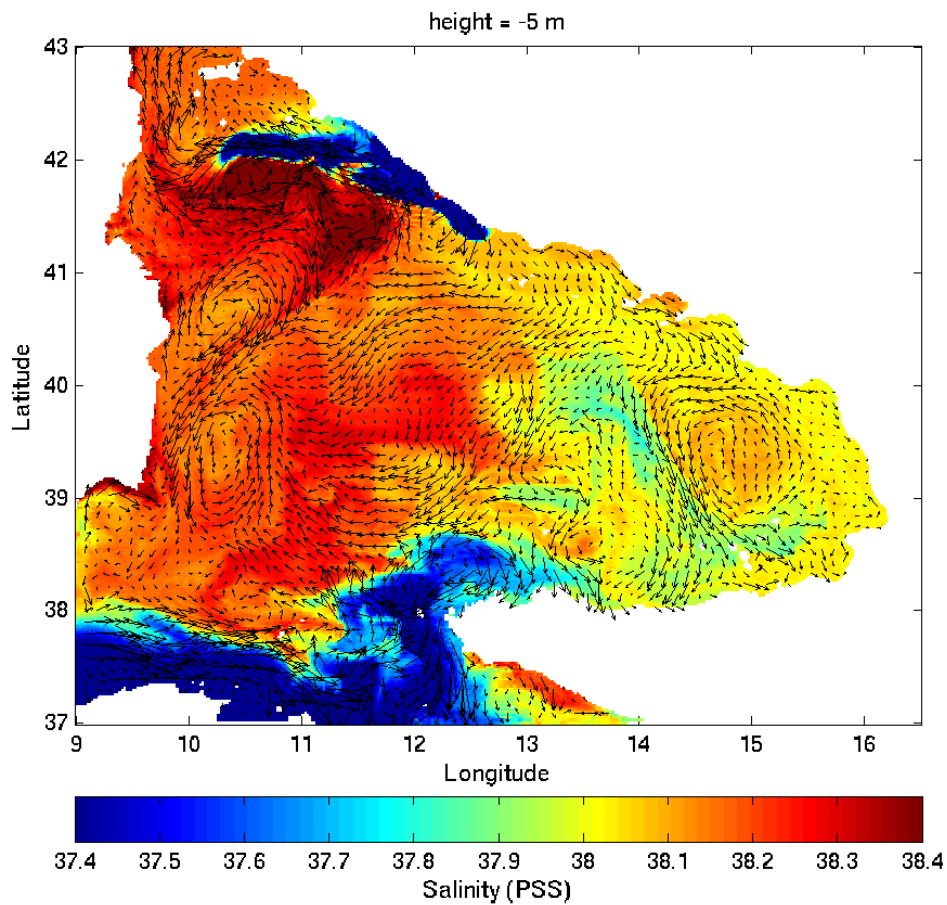


Fig. 11. 12 January 2010, salinity at -5 m .

Evaluation of Tiber river pollutant dispersion in the Tyrrhenian Sea

R. Inghilesi et al.

Title Page

Abstract Introduction

Conclusions References

Tables Figures

⏪ ⏩

◀ ▶

Back Close

Full Screen / Esc

Printer-friendly Version

Interactive Discussion



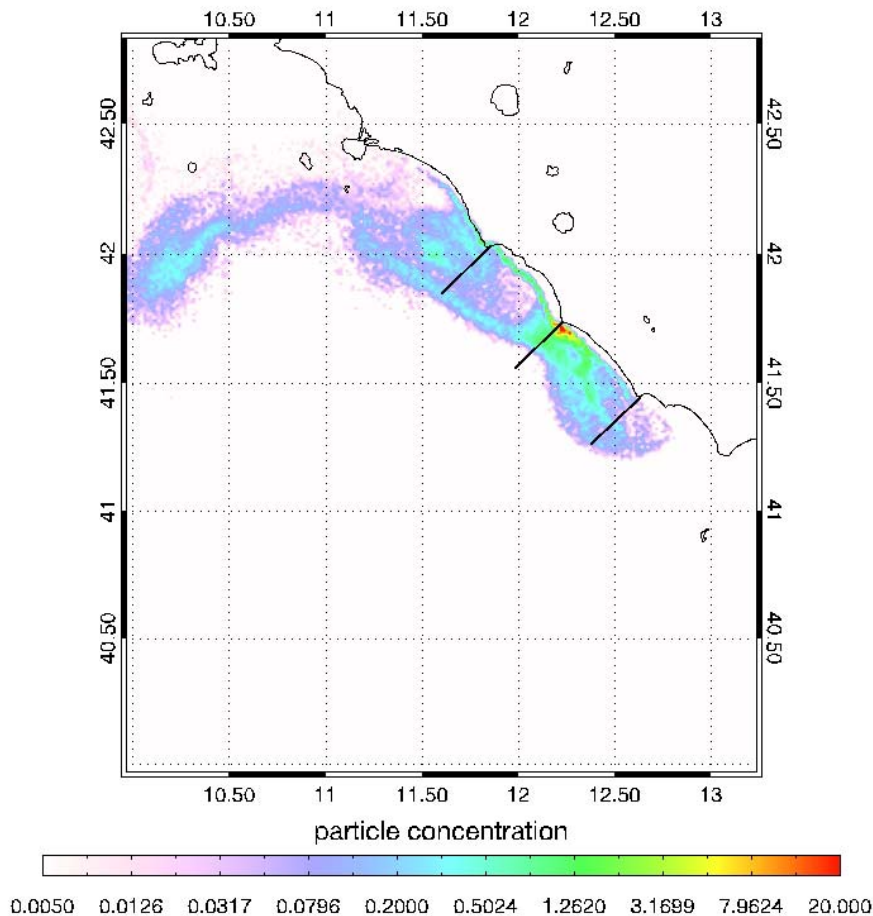


Fig. 12. 12 January 2010, particle dispersion.

Evaluation of Tiber river pollutant dispersion in the Tyrrhenian Sea

R. Inghilesi et al.

Title Page

Abstract

Introduction

Conclusions

References

Tables

Figures

⏪

⏩

◀

▶

Back

Close

Full Screen / Esc

Printer-friendly Version

Interactive Discussion

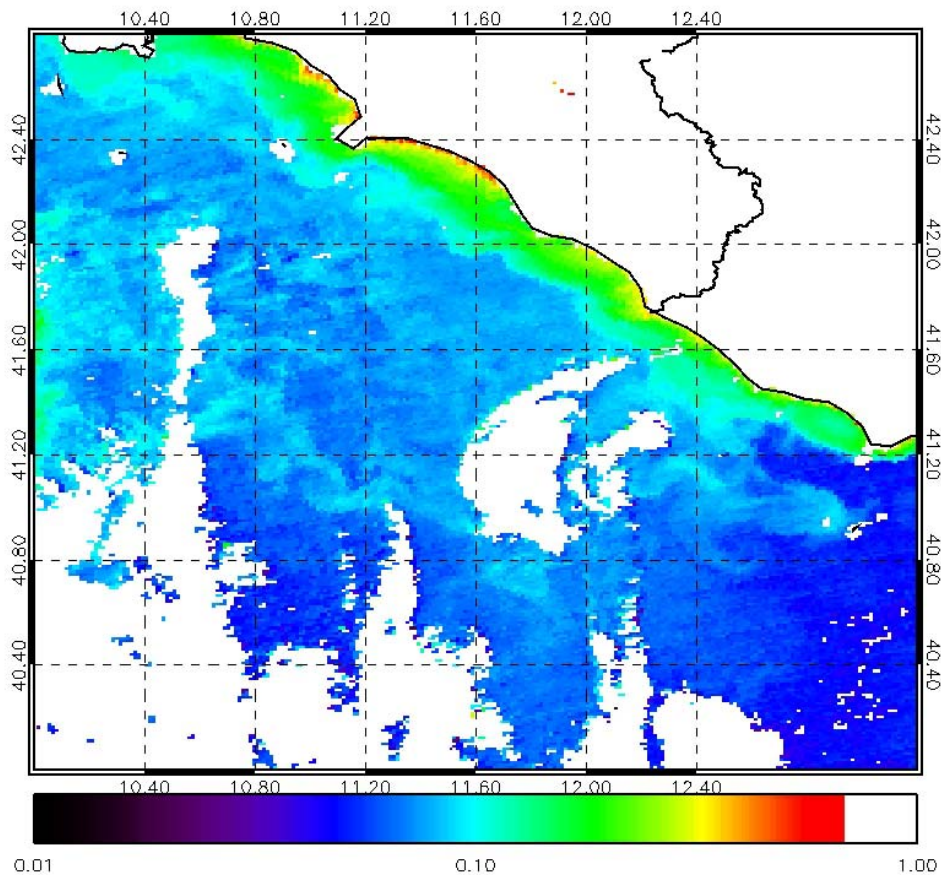


Fig. 13. 16 January 2010, K490 coefficient.

Evaluation of Tiber river pollutant dispersion in the Tyrrhenian Sea

R. Inghilesi et al.

Title Page	
Abstract	Introduction
Conclusions	References
Tables	Figures
◀	▶
◀	▶
Back	Close
Full Screen / Esc	
Printer-friendly Version	
Interactive Discussion	



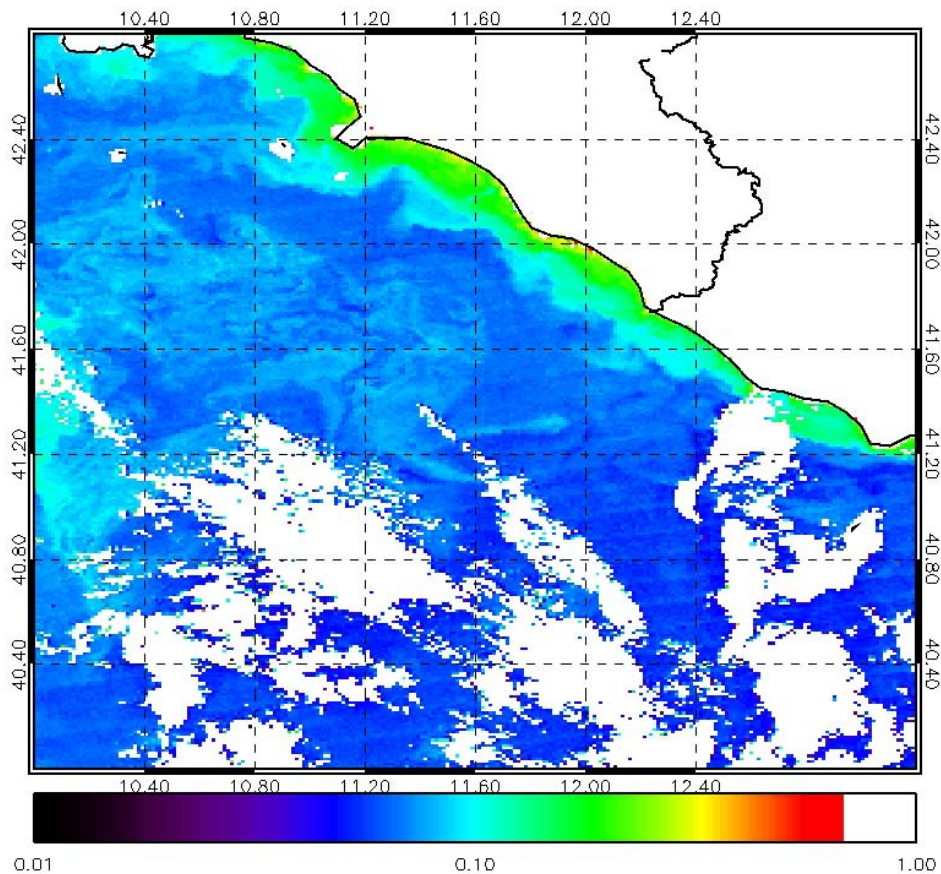


Fig. 14. 19 January 2010, K490 coefficient.

Evaluation of Tiber river pollutant dispersion in the Tyrrhenian Sea

R. Inghilesi et al.

Title Page	
Abstract	Introduction
Conclusions	References
Tables	Figures
⏪	⏩
◀	▶
Back	Close
Full Screen / Esc	
Printer-friendly Version	
Interactive Discussion	



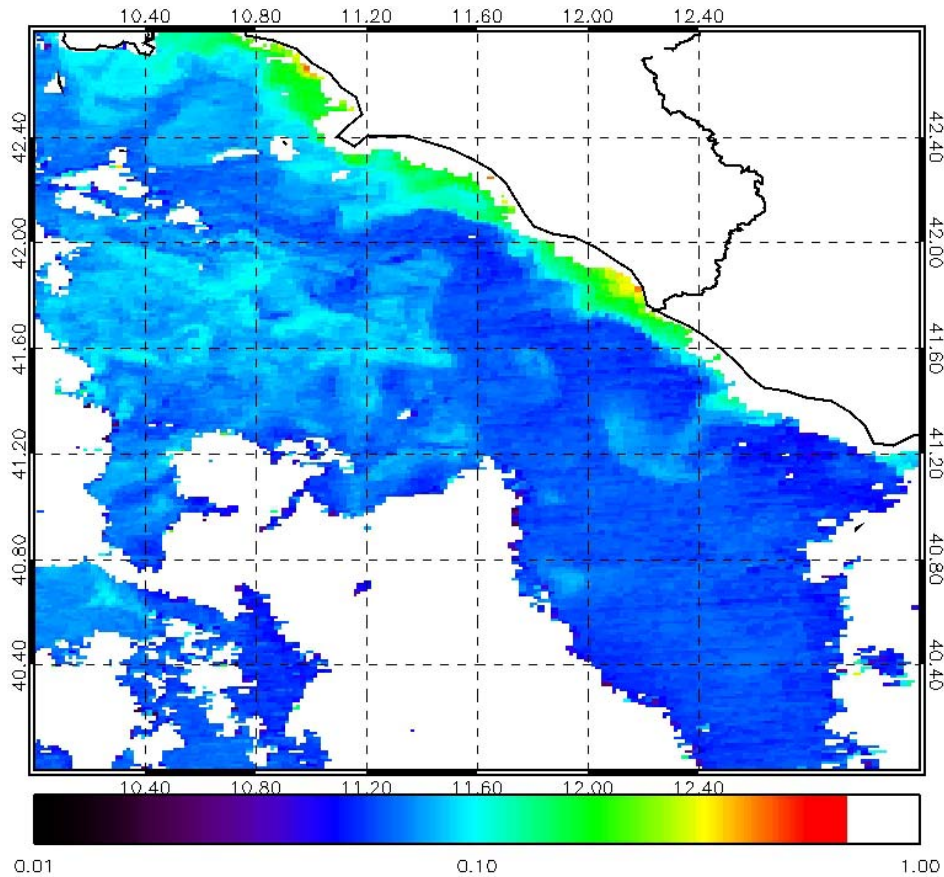


Fig. 15. 22 January 2010, K490 coefficient.

Evaluation of Tiber river pollutant dispersion in the Tyrrhenian Sea

R. Inghilesi et al.

Title Page	
Abstract	Introduction
Conclusions	References
Tables	Figures
⏪	⏩
◀	▶
Back	Close
Full Screen / Esc	
Printer-friendly Version	
Interactive Discussion	



Evaluation of Tiber river pollutant dispersion in the Tyrrhenian Sea

R. Inghilesi et al.

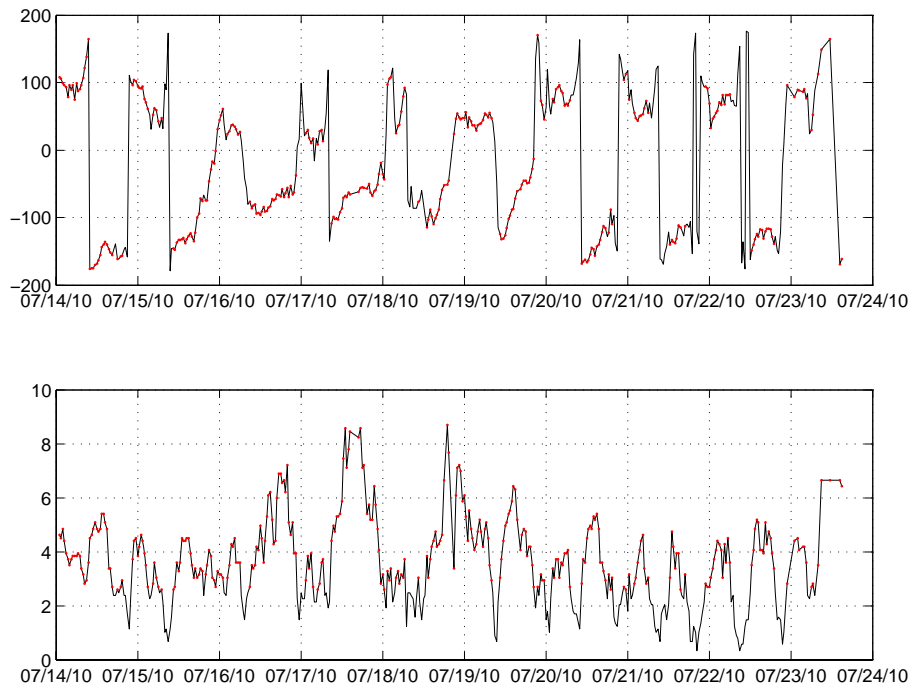


Fig. 16. Offshore wind recorded at the RON buoy of Civitavecchia 14–24 July. **(a)** wind direction **(b)** wind speed red dots indicate wind speed greater than 2.5 m s^{-1} .

[Title Page](#)[Abstract](#)[Introduction](#)[Conclusions](#)[References](#)[Tables](#)[Figures](#)[◀](#)[▶](#)[◀](#)[▶](#)[Back](#)[Close](#)[Full Screen / Esc](#)[Printer-friendly Version](#)[Interactive Discussion](#)

Evaluation of Tiber river pollutant dispersion in the Tyrrhenian Sea

R. Inghilesi et al.

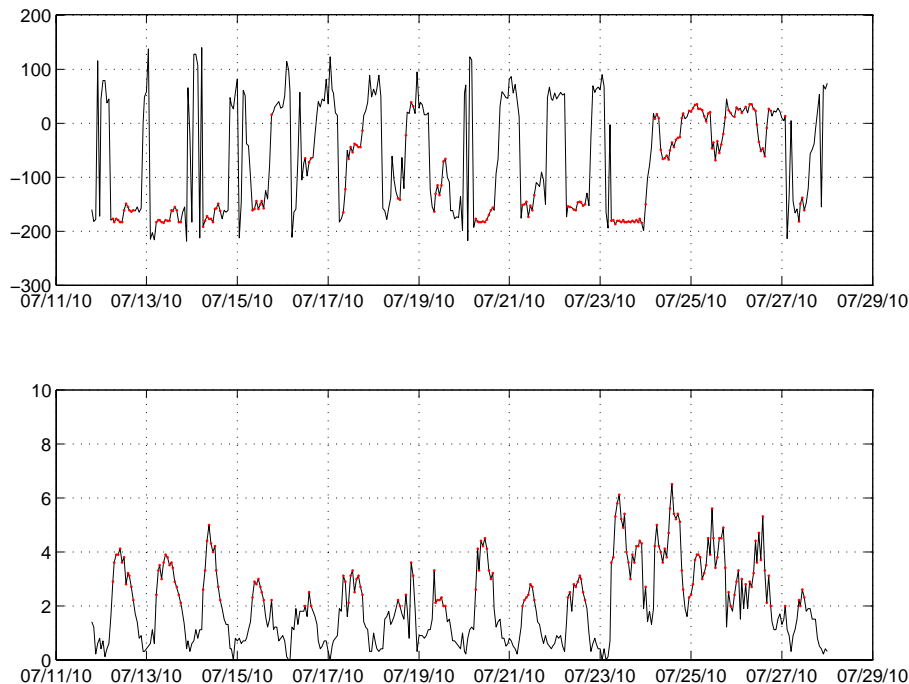


Fig. 17. Onshore wind recorded at the RMN station of Civitavecchia 12–28 July. **(a)** wind direction **(b)** wind speed red dots indicate wind speed greater than 2.5 m s^{-1} .

[Title Page](#)[Abstract](#)[Introduction](#)[Conclusions](#)[References](#)[Tables](#)[Figures](#)[◀](#)[▶](#)[◀](#)[▶](#)[Back](#)[Close](#)[Full Screen / Esc](#)[Printer-friendly Version](#)[Interactive Discussion](#)

Evaluation of Tiber river pollutant dispersion in the Tyrrhenian Sea

R. Inghilesi et al.

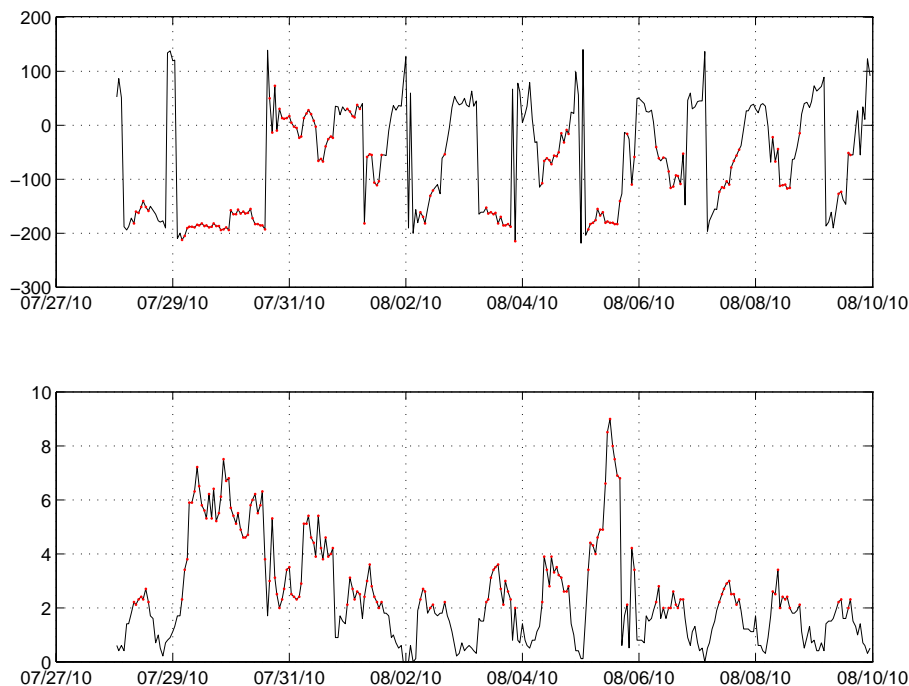


Fig. 18. Onshore wind recorded at the RMN station of Civitavecchia 29 July–10 August (**a**) wind direction (**b**) wind speed red dots indicate wind speed greater than 2.5 m s^{-1} .

[Title Page](#)[Abstract](#)[Introduction](#)[Conclusions](#)[References](#)[Tables](#)[Figures](#)[⏪](#)[⏩](#)[◀](#)[▶](#)[Back](#)[Close](#)[Full Screen / Esc](#)[Printer-friendly Version](#)[Interactive Discussion](#)

Poseidon surface wind (m) 15Z24JUL2010

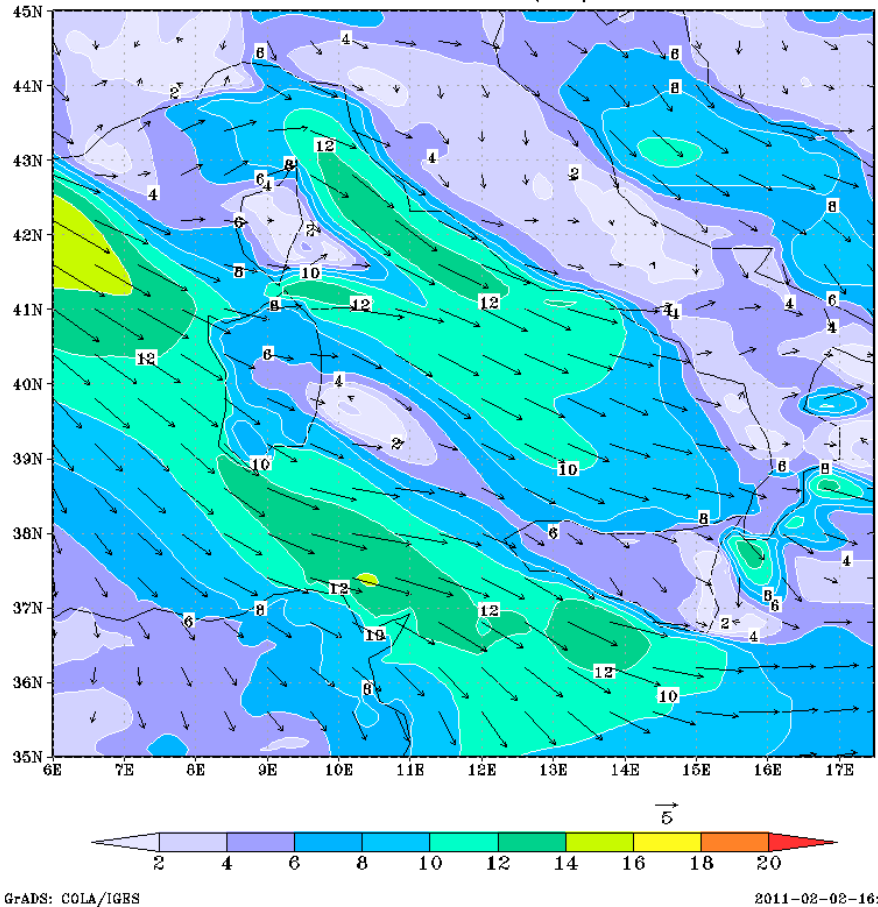


Fig. 19. 24 July 2010, BOLAM wind at the surface.

Evaluation of Tiber river pollutant dispersion in the Tyrrhenian Sea

R. Inghilesi et al.

Title Page

Abstract

Introduction

Conclusions

References

Tables

Figures

◀

▶

◀

▶

Back

Close

Full Screen / Esc

Printer-friendly Version

Interactive Discussion

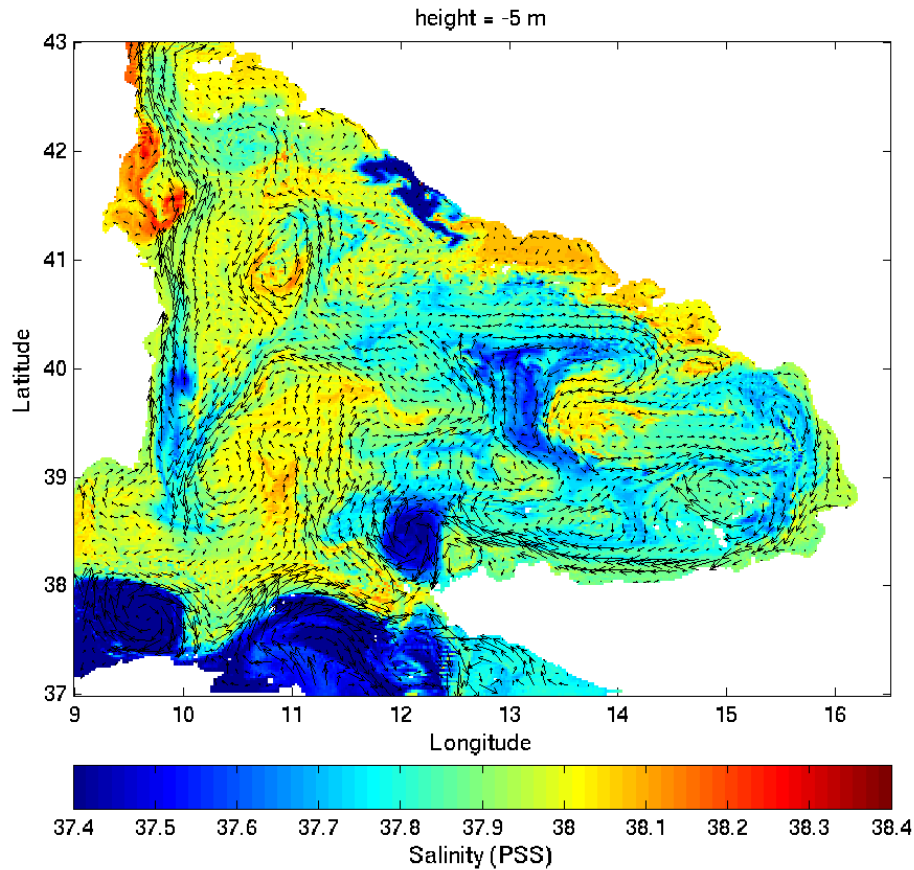


Fig. 20. 14 July 2010, salinity at -5 m.

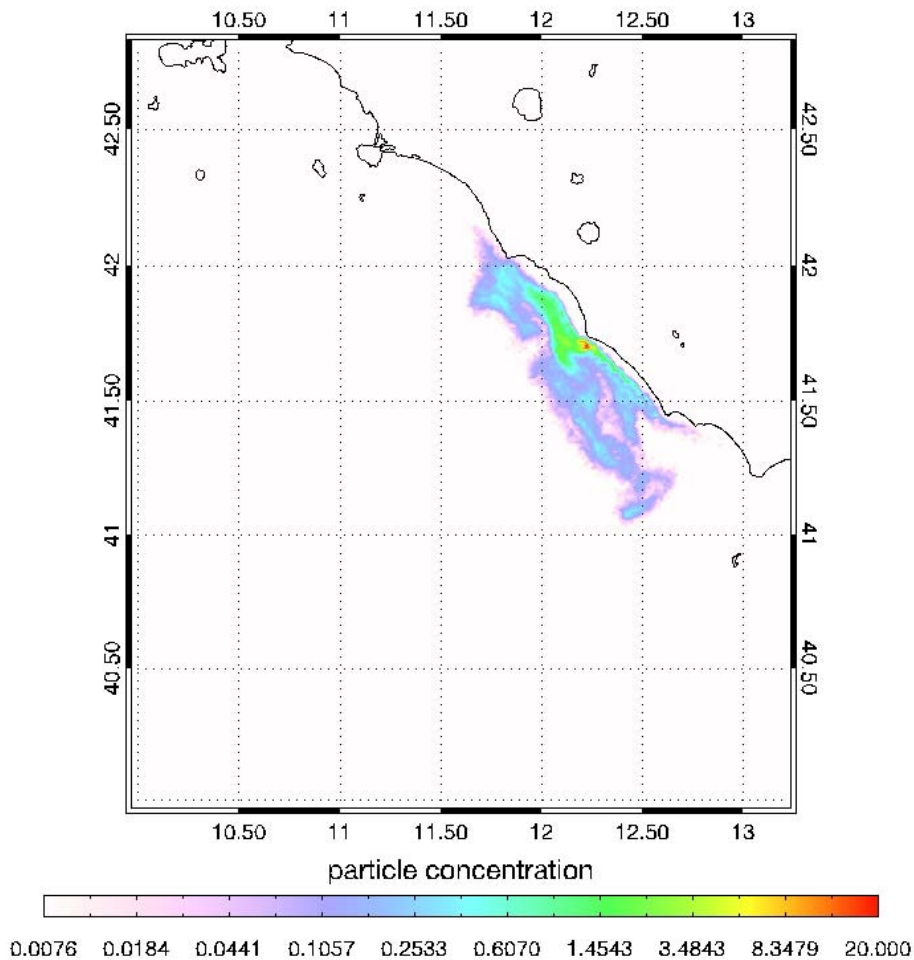


Fig. 21. 14 July 2010, particle dispersion.

Evaluation of Tiber river pollutant dispersion in the Tyrrhenian Sea

R. Inghilesi et al.

Title Page

Abstract

Introduction

Conclusions

References

Tables

Figures

⏪

⏩

◀

▶

Back

Close

Full Screen / Esc

Printer-friendly Version

Interactive Discussion



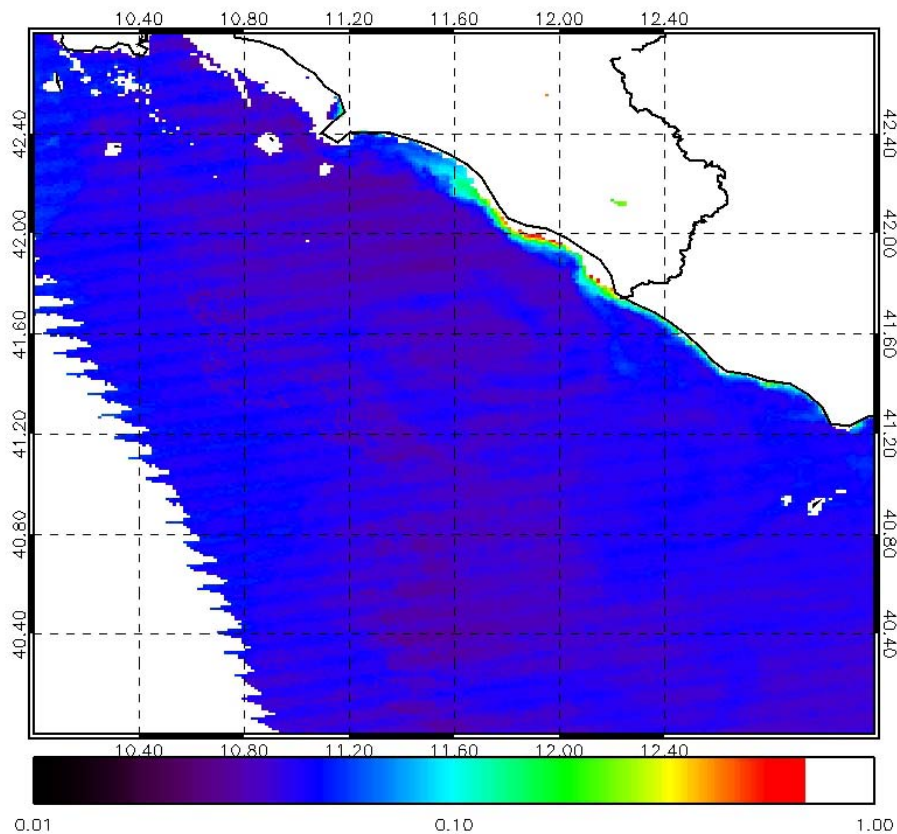


Fig. 22. 14 July 2010, K490 coefficient.

Evaluation of Tiber river pollutant dispersion in the Tyrrhenian Sea

R. Inghilesi et al.

Title Page

Abstract

Introduction

Conclusions

References

Tables

Figures



Back

Close

Full Screen / Esc

Printer-friendly Version

Interactive Discussion



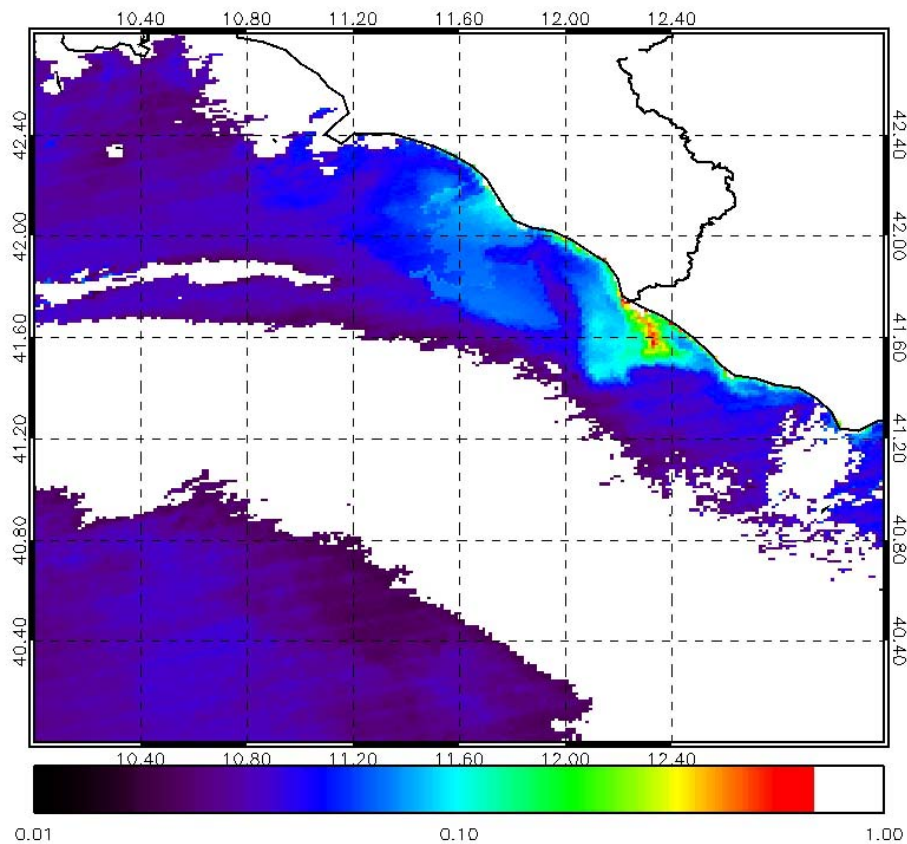


Fig. 23. 18 July 2010, $K490 \text{ m}^{-1}$.

Evaluation of Tiber river pollutant dispersion in the Tyrrhenian Sea

R. Inghilesi et al.

Title Page	
Abstract	Introduction
Conclusions	References
Tables	Figures
⏪	⏩
◀	▶
Back	Close
Full Screen / Esc	
Printer-friendly Version	
Interactive Discussion	



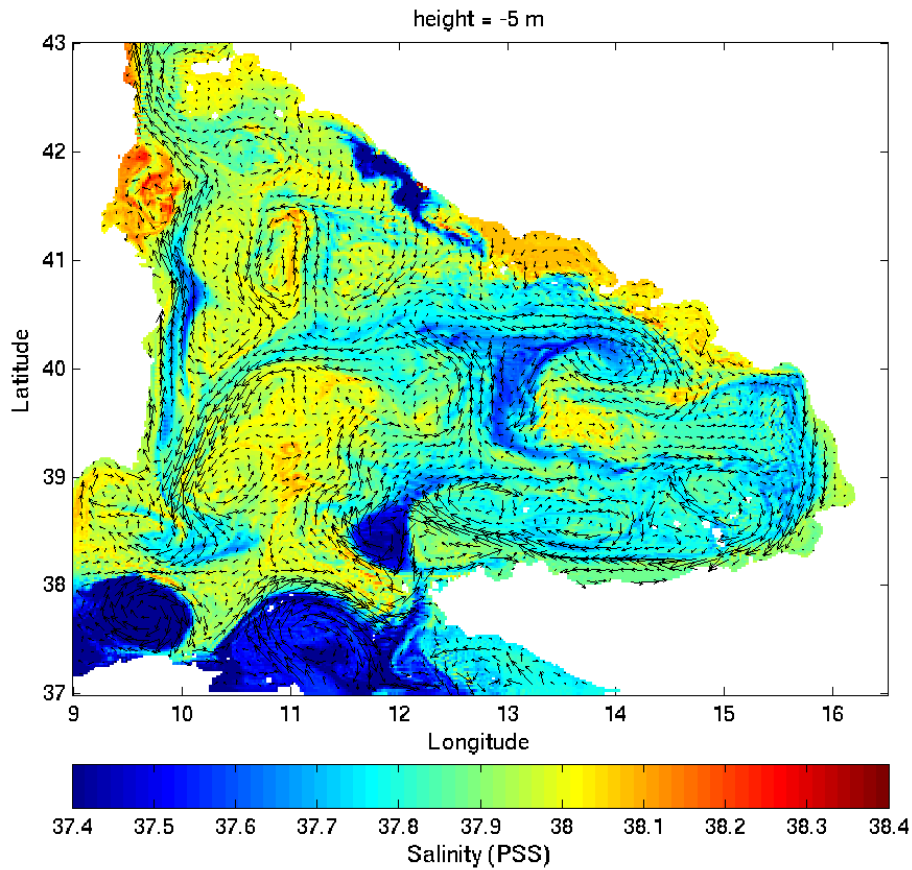


Fig. 24. 18 July 2010, salinity at -5 m.

Evaluation of Tiber river pollutant dispersion in the Tyrrhenian Sea

R. Inghilesi et al.

Title Page

Abstract	Introduction
Conclusions	References
Tables	Figures

⏪	⏩
◀	▶
Back	Close

Full Screen / Esc

Printer-friendly Version

Interactive Discussion

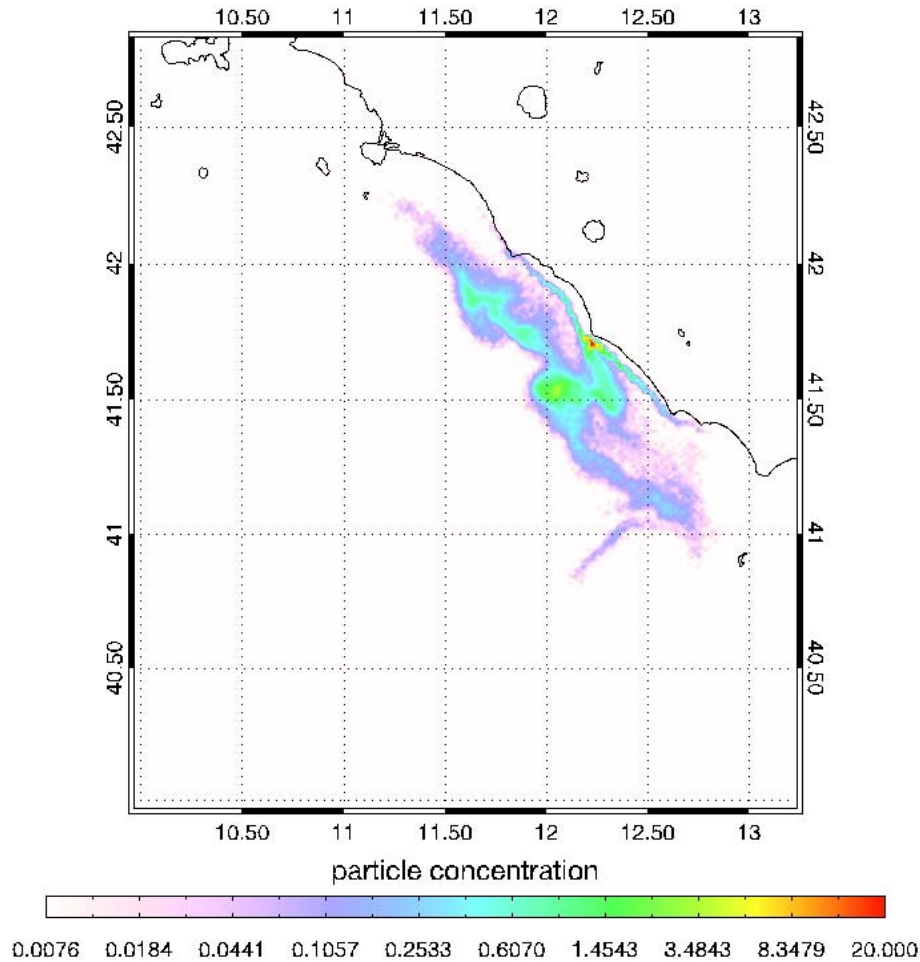


Fig. 25. 18 July 2010, particle dispersion.

Evaluation of Tiber river pollutant dispersion in the Tyrrhenian Sea

R. Inghilesi et al.

Title Page

Abstract

Introduction

Conclusions

References

Tables

Figures

⏪

⏩

◀

▶

Back

Close

Full Screen / Esc

Printer-friendly Version

Interactive Discussion

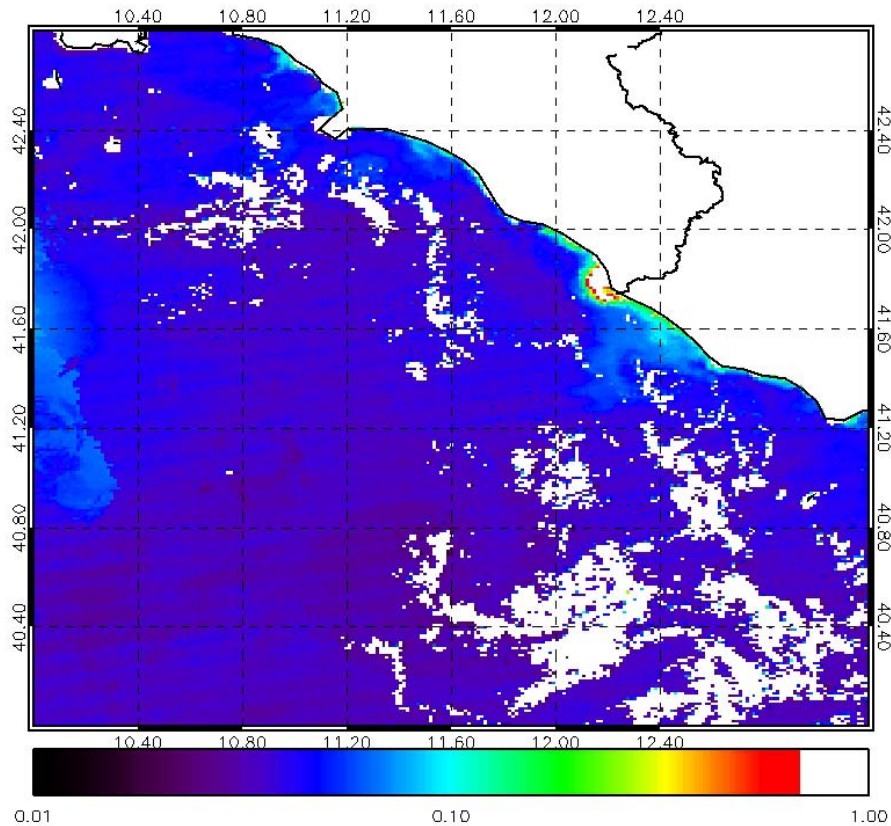


Fig. 26. 21 July 2010, $K490 \text{ m}^{-1}$.

Evaluation of Tiber river pollutant dispersion in the Tyrrhenian Sea

R. Inghilesi et al.

Title Page	
Abstract	Introduction
Conclusions	References
Tables	Figures
◀	▶
◀	▶
Back	Close
Full Screen / Esc	
Printer-friendly Version	
Interactive Discussion	



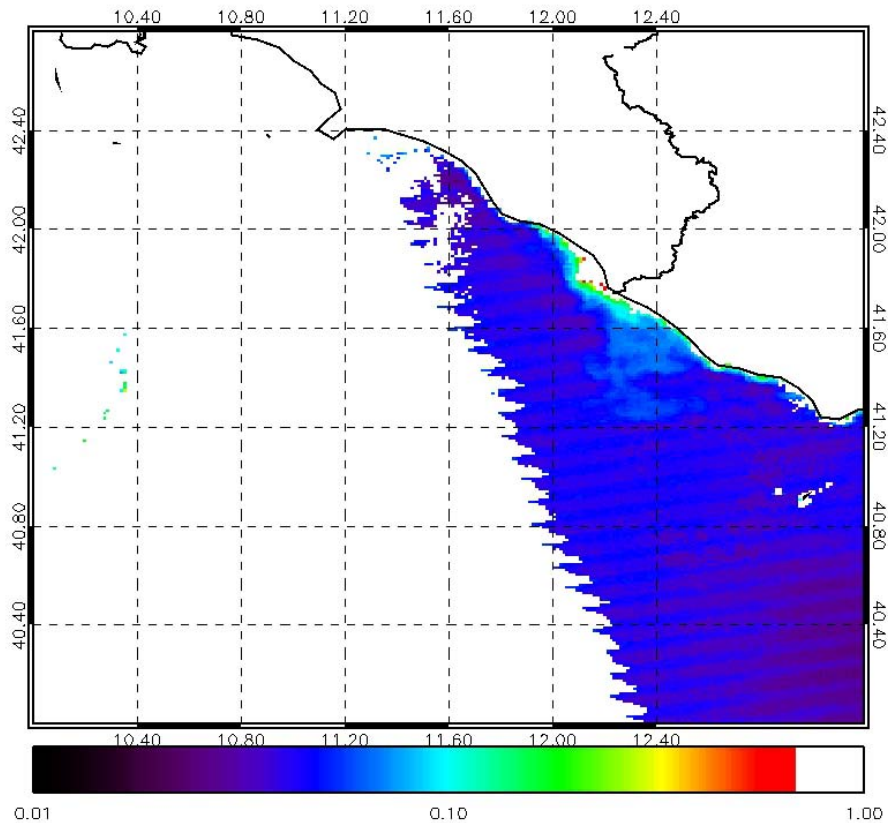


Fig. 27. 23 July 2010, K490 m⁻¹.

Evaluation of Tiber river pollutant dispersion in the Tyrrhenian Sea

R. Inghilesi et al.

Title Page

Abstract Introduction

Conclusions References

Tables Figures

⏪ ⏩

⏴ ⏵

Back Close

Full Screen / Esc

Printer-friendly Version

Interactive Discussion



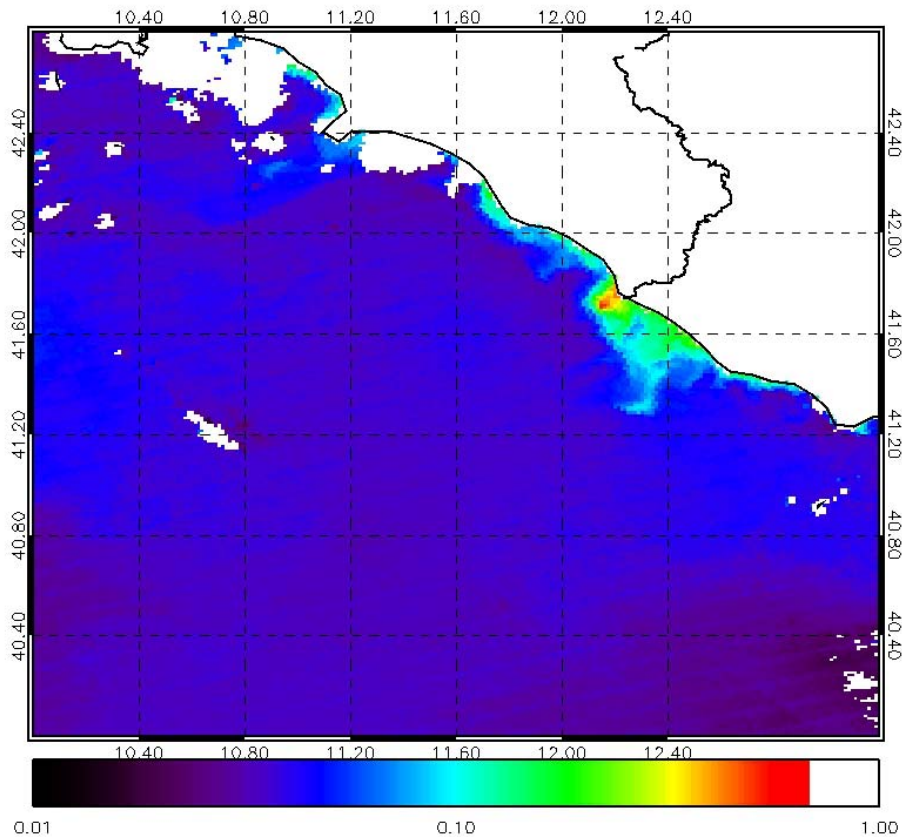


Fig. 28. 27 July 2010, K490 coefficient.

Evaluation of Tiber river pollutant dispersion in the Tyrrhenian Sea

R. Inghilesi et al.

Title Page

Abstract Introduction

Conclusions References

Tables Figures

⏪ ⏩

⏴ ⏵

Back Close

Full Screen / Esc

Printer-friendly Version

Interactive Discussion



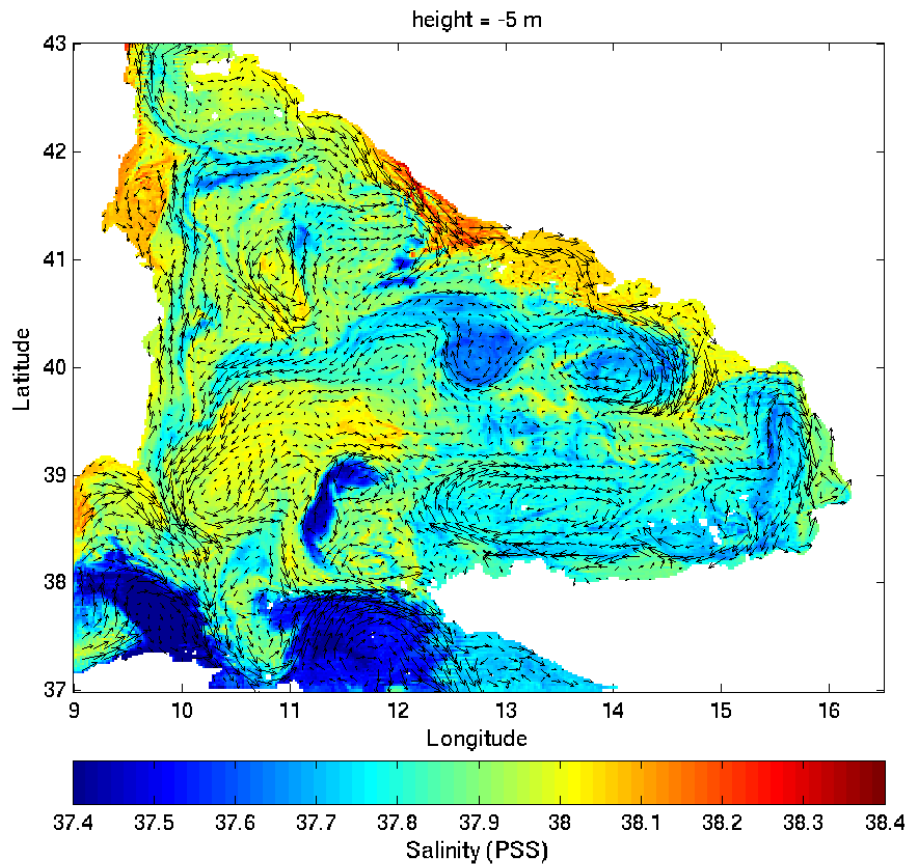


Fig. 29. 27 July 2010, salinity at -5 m.

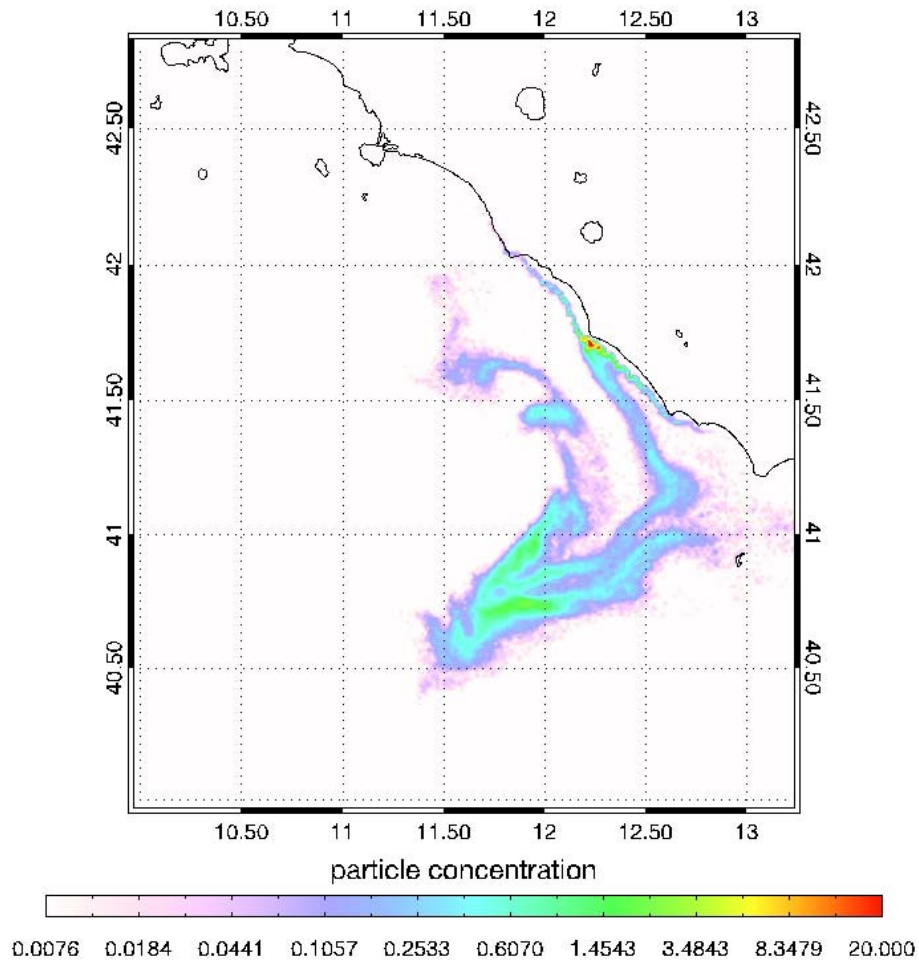


Fig. 30. 27 July 2010, particle dispersion.

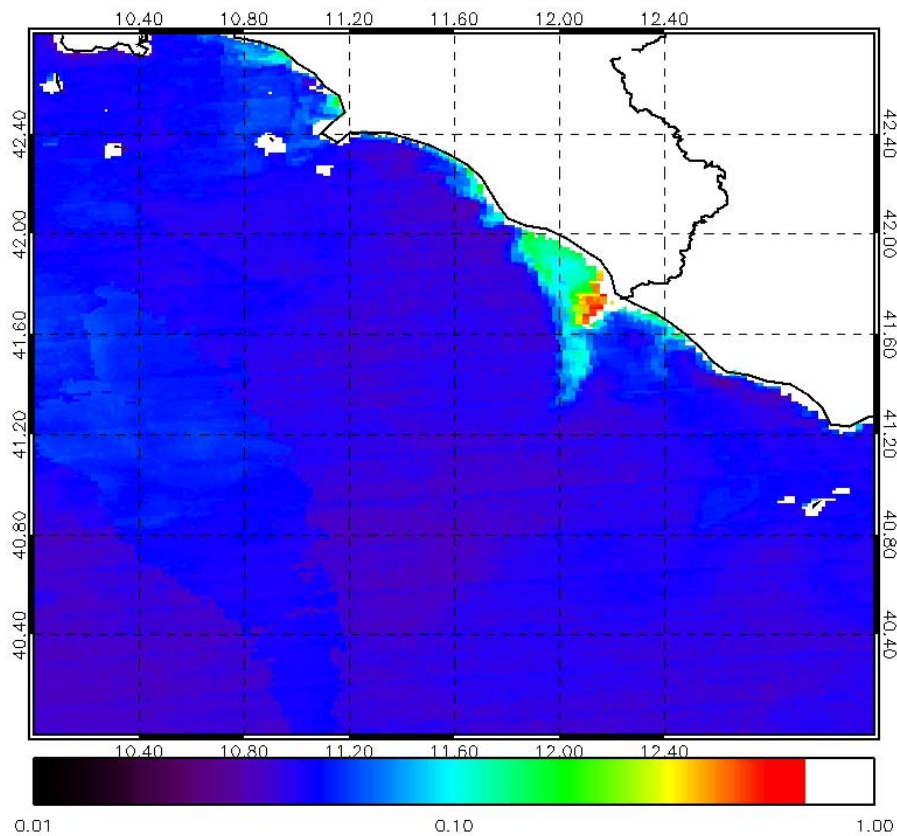


Fig. 31. 2 August 2010, $K490 \text{ m}^{-1}$.

Evaluation of Tiber river pollutant dispersion in the Tyrrhenian Sea

R. Inghilesi et al.

Title Page

Abstract Introduction

Conclusions References

Tables Figures

⏪ ⏩

◀ ▶

Back Close

Full Screen / Esc

Printer-friendly Version

Interactive Discussion

